

Quantifying Environmental Control on Tropical Cyclone Intensity Change

ERIC A. HENDRICKS AND MELINDA S. PENG

Marine Meteorology Division, Naval Research Laboratory, Monterey, California

BING FU AND TIM LI

Department of Meteorology, and International Pacific Research Center, University of Hawaii at Manoa, Honolulu, Hawaii

(Manuscript received 5 August 2009, in final form 16 February 2010)

ABSTRACT

Composite analysis is used to examine environmental and climatology and persistence characteristics of tropical cyclones (TCs) undergoing different intensity changes in the western North Pacific (WPAC) and North Atlantic (ATL) ocean basins. Using the cumulative distribution functions of 24-h intensity changes from the 2003–08 best-track data, four intensity change bins are defined: rapidly intensifying (RI), intensifying, neutral, and weakening. The Navy Operational Global Atmospheric Prediction System daily 0000 and 1200 UTC global analysis and Tropical Rainfall Measuring Mission Microwave Imager data are then used as proxies for the real atmosphere, and composites of various environmental fields believed relevant to TC intensity change are made in the vicinity of the TCs. These composites give the average characteristics near the TC, prior to undergoing a given intensity change episode.

For the environmental variables, statistically significant differences are examined between RI storms and the other groups. While some environmental differences were found between RI and weakening/neutral TCs in both basins, an interesting result from this study is that the environment of RI TCs and intensifying TCs is quite similar. This indicates that the rate of intensification is only weakly dependent on the environmental conditions, on average, provided the environment is favorable. Notable exceptions were that in the WPAC, RI events occurred in environments with significantly larger conditional instability than intensifying events. In the ATL, RI events occurred in environments with weaker deep-layer shear than intensifying events. An important finding of this work is that SSTs are similar between intensifying and rapidly intensifying TCs, indicating that the rate of intensification is not critically dependent on SST.

The TCs in both basins were more intense prior to undergoing an RI episode than an intensifying or neutral episode. In the WPAC, the three groups had similar translational speeds and headings, and average initial position. In the ATL, RI storms were located farther south than intensifying and neutral storms, and had a larger translational speed and a more westward component to the heading.

1. Introduction

With regard to tropical cyclone (TC) intensity, there are two important questions: (i) what is the maximum intensity a TC may achieve in a given environment, and (ii) at what rate will a TC change its intensity in that environment? The former question has largely been answered by maximum potential intensity (MPI) theories (Emanuel 1986, 1988; Holland 1997). The latter question is much more problematic. Intensity change can be defined as $\partial V_{\max}/\partial t$ or $\partial p_{\min}/\partial t$, where V_{\max} is the maximum

sustained surface wind and p_{\min} is the minimum central pressure. These instantaneous derivatives can fluctuate because of a variety of factors in the environment and ocean, as well as internal processes occurring inside the storm. Examples of the former are the deep-layer vertical wind shear, sea surface temperature (SST), interactions with upper-level troughs, and the level of conditional instability in the lower troposphere. Examples of the latter include eyewall replacement cycles, potential vorticity (PV) mixing between eye and eyewall, and convectively coupled vortex Rossby waves [see the review article by Wang and Wu (2004) for concise review of all known factors governing hurricane intensity change]. Note that microphysical processes, including hydrometeor production and latent heat release, may also be

Corresponding author address: Eric A. Hendricks, Naval Research Laboratory, Monterey, CA 93940.
E-mail: eric.hendricks@nrlmry.navy.mil

Report Documentation Page

Form Approved
OMB No. 0704-0188

Public reporting burden for the collection of information is estimated to average 1 hour per response, including the time for reviewing instructions, searching existing data sources, gathering and maintaining the data needed, and completing and reviewing the collection of information. Send comments regarding this burden estimate or any other aspect of this collection of information, including suggestions for reducing this burden, to Washington Headquarters Services, Directorate for Information Operations and Reports, 1215 Jefferson Davis Highway, Suite 1204, Arlington VA 22202-4302. Respondents should be aware that notwithstanding any other provision of law, no person shall be subject to a penalty for failing to comply with a collection of information if it does not display a currently valid OMB control number.

1. REPORT DATE

FEB 2010

2. REPORT TYPE

3. DATES COVERED

00-00-2010 to 00-00-2010

4. TITLE AND SUBTITLE

Quantifying Environmental Control on Tropical Cyclone Intensity Change

5a. CONTRACT NUMBER

5b. GRANT NUMBER

5c. PROGRAM ELEMENT NUMBER

6. AUTHOR(S)

5d. PROJECT NUMBER

5e. TASK NUMBER

5f. WORK UNIT NUMBER

7. PERFORMING ORGANIZATION NAME(S) AND ADDRESS(ES)

Naval Research Laboratory, Marine Meteorology Division, Monterey, CA, 93943

8. PERFORMING ORGANIZATION REPORT NUMBER

9. SPONSORING/MONITORING AGENCY NAME(S) AND ADDRESS(ES)

10. SPONSOR/MONITOR'S ACRONYM(S)

11. SPONSOR/MONITOR'S REPORT NUMBER(S)

12. DISTRIBUTION/AVAILABILITY STATEMENT

Approved for public release; distribution unlimited

13. SUPPLEMENTARY NOTES

14. ABSTRACT

Composite analysis is used to examine environmental and climatology and persistence characteristics of tropical cyclones (TCs) undergoing different intensity changes in the western North Pacific (WPAC) and North Atlantic (ATL) ocean basins. Using the cumulative distribution functions of 24-h intensity changes from the 2003?08 best-track data, four intensity change bins are defined: rapidly intensifying (RI), intensifying neutral, and weakening. The Navy Operational Global Atmospheric Prediction System daily 0000 and 1200 UTC global analysis and Tropical Rainfall Measuring Mission Microwave Imager data are then used as proxies for the real atmosphere, and composites of various environmental fields believed relevant to TC intensity change are made in the vicinity of the TCs. These composites give the average characteristics near the TC, prior to undergoing a given intensity change episode. For the environmental variables, statistically significant differences are examined between RI storms and the other groups. While some environmental differences were found between RI and weakening/neutral TCs in both basins, an interesting result from this study is that the environment of RI TCs and intensifying TCs is quite similar. This indicates that the rate of intensification is only weakly dependent on the environmental conditions, on average, provided the environment is favorable. Notable exceptions were that in the WPAC RI events occurred in environments with significantly larger conditional instability than intensifying events. In the ATL, RI events occurred in environments with weaker deep-layer shear than intensifying events. An important finding of this work is that SSTs are similar between intensifying and rapidly intensifying TCs indicating that the rate of intensification is not critically dependent on SST. The TCs in both basins were more intense prior to undergoing an RI episode than an intensifying or neutral episode. In the WPAC, the three groups had similar translational speeds and headings, and average initial position. In the ATL, RI storms were located farther south than intensifying and neutral storms, and had a larger translational speed and a more westward component to the heading.

15. SUBJECT TERMS

16. SECURITY CLASSIFICATION OF:			17. LIMITATION OF ABSTRACT Same as Report (SAR)	18. NUMBER OF PAGES 29	19a. NAME OF RESPONSIBLE PERSON
a. REPORT unclassified	b. ABSTRACT unclassified	c. THIS PAGE unclassified			

Standard Form 298 (Rev. 8-98)
Prescribed by ANSI Std Z39-18

included in internal dynamics. Scale interactions are also prominent in TC evolution, such as large-scale vertical wind shear inducing vorticity asymmetries in the inner core, affecting structure and intensity. Because of the complexity of TC intensity change, intensity forecast skill improvement has continued to lag track skill improvement (e.g., DeMaria et al. 2007). Moreover, there is poor intensity guidance in multiple phases of the TC life cycle, including transition from a tropical depression to a tropical storm, rapid intensification and decay, and fluctuations when a storm is near its maximum intensity (Elsberry et al. 2007).

Recently there has been considerable interest in understanding the physical and dynamical processes responsible for rapid intensification (RI), which is usually defined as the 95th percentile of all 24-h over-water intensity changes, corresponding to approximately $+15 \text{ m s}^{-1}$ or greater (Kaplan and DeMaria 2003). Since RI is observed to be highly unpredictable, a natural null hypothesis is that RI must be primarily driven by internal dynamics. To state this in another way, while global models have steadily improved in their ability to predict the large-scale environmental conditions, more accurate knowledge of the environment has not resulted in significant improvement in RI (or intensity) forecast skill. There have been a number of studies in RI that emphasized both the environment, internal dynamics, or a combination of both. Examining TC Opal (1995), Bosart et al. (2000) found that RI was initiated by an interaction with a trough with upper-level divergence, creating enhanced convective activity in the inner core. For the same case, Persing et al. (2002) argued the trough played a minimal role, and Hong et al. (2000) found that the warm core ring in which Opal moved over was critical in its RI. The role of warm ocean anomalies in RI has also been emphasized recently by Lin et al. (2009) and Mainelli et al. (2008). Schubert et al. (1999), Kossin and Schubert (2001), and Hendricks et al. (2009) have found that large pressure falls may occur during mixing of PV between the eye and eyewall resulting from barotropic instability of the eyewall PV ring. Recently, Vigh and Schubert (2009) found that the warm core in TCs may rapidly develop if a portion of the deep convection occurs inside the radius of maximum wind. Reasor et al. (2009) examined RI in a sheared hurricane and found that asymmetric convection induced by the shear was crucial for RI. Rogers (2010) and Guimond et al. (2010) also emphasize the importance of hot towers and convective bursts in rapid intensification. The resulting viewpoint is that there are multiple pathways to RI, and RI can sometimes happen in less than ideal environments because of favorable internal dynamics. In an effort to better understand the large-scale characteristics

of RI storms, Kaplan and DeMaria (2003) performed a systematic study in the North Atlantic basin comparing the conditions of TCs that underwent RI episodes to those that did not (non RI). The main conclusions of their work are as follows: (i) RI cases happen farther south and west in geographic location than non-RI cases and have more westward component of motion, (ii) RI cases are farther from their maximum potential intensity, (iii) RI cases happen in warmer SSTs and greater lower-tropospheric relative humidity than non-RI, and (iv) RI cases happen in weaker deep-layer vertical wind shear and where the upper-level flow is more easterly.

The purpose of the present work is to objectively quantify environmental control on TC intensity change, and in particular, rapid intensification. Using the Joint Typhoon Warning Center (JTWC) and National Hurricane Center (NHC) best-track cumulative distribution functions of 24-h intensity changes from 2003 to 2008, we define four separate intensity change bins in the North Atlantic (ATL) and western North Pacific (WPAC) basins: (i) rapidly intensifying, (ii) intensifying, (iii) neutral, and (iv) weakening. Then the Navy Operational Global Atmospheric Prediction System (NOGAPS; Hogan and Rosmond 1991) twice-daily global analysis and Tropical Rainfall Measuring Mission (TRMM) Microwave Imager (TMI) data are used to create the composite environment around the TC for each intensity change bin. Using these composites, we will show the characteristics that differentiate intensifying versus weakening TCs, as well the characteristics that differentiate intensifying versus rapidly intensifying TCs. Additionally, a comparison of these characteristics will be made between the two ocean basins. In section 2, the data and methods for the study are described. In section 3, the composites of the atmospheric variables and SSTs are presented to obtain qualitative information on the variance in the environment for different intensity change bins. In section 4, a synthesis of the composite results is presented, along with statistical tests that quantify differences between intensity change groups. In section 5, the variability in environmental parameters for rapidly intensifying TCs is assessed. Finally, the main conclusions of this study are given in section 6.

2. Data and methods

a. Data used

The data used in this study are: (i) NOGAPS daily 0000 and 1200 UTC global analysis, (ii) JTWC and NHC (Jarvinen et al. 1984) best-track data, and (iii) TMI data. All data were collected for the period 2003–08. The NOGAPS global analysis is at $1^\circ \times 1^\circ$ horizontal

resolution with 21 pressure levels from 1013 to 10 hPa (with finer vertical resolution near the surface). The analysis used is an operational analysis, and it is produced using a first guess from the forecast model along with three-dimensional variational data assimilation (Daley and Barker 2001). As an operational forecast system, NOGAPS has been upgraded continually in model resolution and physics. Some important operational improvements since 2003 were the direct assimilation of satellite radiances and improvements to the cumulus parameterization (Peng et al. 2004). The JTWC and NHC best-track data represents the best estimate of the TC intensity based on all available data at the analysis time, which includes satellite-derived estimates (Dvorak 1975, 1984) and also aircraft reconnaissance data, if available. The intensity is given as a minimum central pressure and maximum sustained wind estimate, and it is recorded 4 times per day: at 0000, 0600, 1200, and 1800 UTC. The TMI is passive microwave imager on board the TRMM satellite that has a semi-equatorial orbit. Sea surface temperature retrievals are obtained at 10.7 GHz, allowing the sensor to see through clouds. The TMI version 4 product was obtained from the Remote Sensing Systems Web site (see online at <http://www.ssmi.com/tmi>). More details on the retrieval can be found in Hilburn and Wentz (2008). The data are at a horizontal resolution of 0.25° and their coverage extends from 40°S to 40°N . The data contains SST, water vapor, cloud liquid water, rain-rate, and surface wind measurements. For this study, the SST and rain-rate data were used.

b. Selection of intensity change bins

The 0000 and 1200 UTC best-track intensity estimates were used to correspond to the global analysis time levels. The maximum sustained wind was chosen as the intensity metric. The best-track data were filtered so that only records of tropical depression intensity or stronger were retained. Using the best-track data, +24 h (24 h into the future) intensity changes were calculated and recorded at each 0000 and 1200 UTC synoptic time. Next, cases in which the TC had any land interaction within +24 h were removed, since we are primarily interested factors governing over-water intensity changes. These land interaction cases included events in which a TC moved over an island and then reemerged into open water in a 24-h time period. Finally, cases where the TC was positioned above 30°N were removed because many of these TCs had extratropical influences. The filtered dataset yielded 732 and 1424 intensity change estimates for the ATL and WPAC basins, respectively. Probability density and cumulative distribution functions for these data are shown in Fig. 1. Note

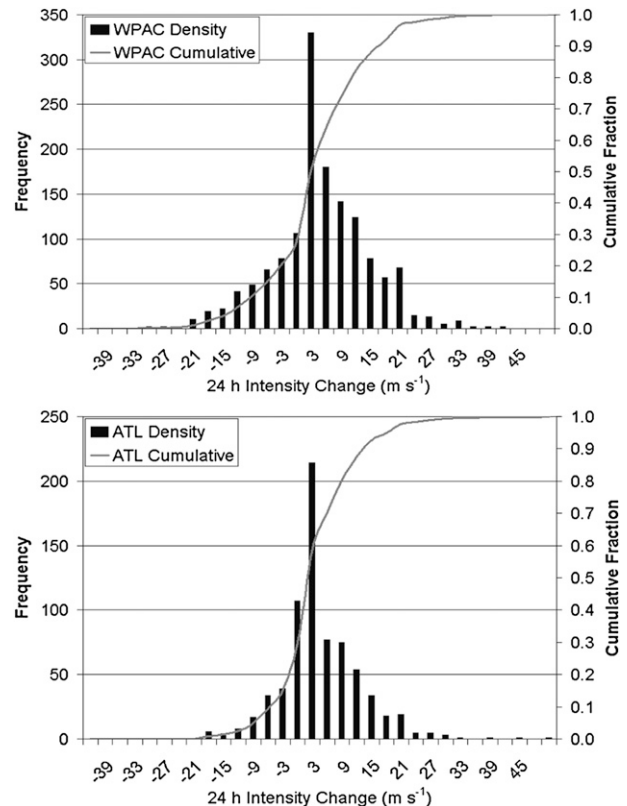


FIG. 1. Probability density and cumulative distribution functions for 2003–08 over-water 24-h intensity changes in the (top) WPAC and (bottom) ATL basins (from JTWC and NHC best-track data).

that the skewness with more intensifying cases than weakening cases is mainly due to the removal of the land interaction cases. Also note that in the ATL, there are three extreme rapidly intensifying events. Two of these events are associated with TC Wilma (2005), which had two RI events of $+48$ and $+38 \text{ m s}^{-1}$. The other event was TC Felix (2007), which had an RI event of $+43 \text{ m s}^{-1}$. In the WPAC, the TC with the largest RI event was TC Chebi (2006; 23°W), which had a RI event of $+41 \text{ m s}^{-1}$. Using the 95th percentile of the cumulative distribution functions, the maximum sustained wind threshold for rapid intensification was determined for each basin. Next, four more intensity change categories were defined using equal-sized bins. The five intensity change categories (rapidly weakening, weakening, neutral, intensifying, and rapidly intensifying), along with the range and sample size for each basin are given in Table 1. A percentage of these samples in each basin are not unique because they occurred sequentially in the same TC. For RI, the ATL had 13 of these events while the WPAC had 24 of these events. The number of unique RI events for the ATL and WPAC basins are 23 and 56, respectively.

TABLE 1. Intensity change categories (ΔV_{\max} within the next 24 h), definitions, and sample sizes for the WPAC and ATL basins.

Category	WPAC range (m s^{-1})	No. of cases	ATL range (m s^{-1})	No. of cases
Rapidly weakening (RW)	$\Delta V_{\max} < -19.5$	20	$\Delta V_{\max} < -18.0$	6
Weakening (W)	$-19.5 \leq \Delta V_{\max} < -6.5$	193	$-18.0 \leq \Delta V_{\max} < -6.0$	63
Neutral (N)	$-6.5 \leq \Delta V_{\max} < +6.5$	694	$-6.0 \leq \Delta V_{\max} < +6.0$	437
Intensifying (I)	$+6.5 \leq \Delta V_{\max} < +19.5$	436	$+6.0 \leq \Delta V_{\max} < +18.0$	181
Rapidly intensifying (RI)	$\Delta V_{\max} \geq +19.5$	81	$\Delta V_{\max} \geq +18.0$	36

c. Composite variable selection

The selection of the atmospheric variables was subjective based from factors that are known to strongly affect TC intensity change. The chosen variables are: deep-layer vertical wind shear, conditional instability in the lower troposphere, moisture content at low and mid-levels, large-scale divergence patterns at low and upper levels, low-level environmental relative vorticity, and SST. The specific definitions of these variables are listed in Table 2. We now briefly review the mechanisms by which these variables modulate TC intensity.

The energy supply for TCs comes from fluxes of latent and sensible heat from the underlying ocean. As the low-level winds become stronger, the evaporation rates increase, leading to increased latent heat fluxes into the storm. Therefore, higher SSTs would be correlated with larger intensification rates, provided disequilibrium exists between the ocean surface and surface layer and notwithstanding other atmospheric factors. However, if a storm is very strong and moves slowly, the upwelling of cooler water would decrease (or even reverse) these fluxes and may cause the storm to weaken (Bender and Ginis 2000). For these storms, coupled ocean–atmosphere models are needed to accurately simulate the intensity. It should be noted, however,

that historically SST has been more connected to determining an upper bound on the intensity of the storm rather than determining the rate of intensification (Emanuel 1986; Merrill 1988b).

The mechanism by which TCs intensify is through deep cumulonimbus convection. In the context of a wind-induced surface heat exchange (WISHE; Emanuel 1986; Rotunno and Emanuel 1987), convection efficiently transports moist entropy from the surface to upper levels in a pseudoadiabatic expansion step of the Carnot heat engine cycle. However, the instability itself depends on positive feedback between the surface winds and heat fluxes, with stronger surface winds increasing sensible and latent heat fluxes into the storm. This is in contrast to conditional instability of the second kind (CISK; Ooyama 1964; Charney and Eliassen 1964), which relies on a cooperative feedback between smaller-scale deep convection and larger-scale circulation. In the latter case, an environment that is more conditionally unstable will favor enhanced convective activity and thus be more conducive for TC intensification. In environments with ample ambient low-level relative vertical vorticity, deep convective hot towers can converge and stretch that vorticity into small-scale lower-tropospheric towers. These vortical hot towers (Hendricks et al. 2004; Montgomery et al. 2006) can generate near-surface convergence in the boundary layer, and also be axisymmetrized

TABLE 2. Composite variables, description, units, and data source. An f in the superscript position denotes that low-pass filtering was applied to the field. Dot and cross products below are calculated in spherical coordinates using a constant Earth radius $a = 6370$ km.

Variable	Description	Units	Data source
Deep-layer shear	$ \mathbf{u}_{200}^f - \mathbf{u}_{850}^f $	m s^{-1}	NOGAPS
Instability	$\partial\theta_E/\partial p$	K Pa^{-1}	NOGAPS
850-hPa divergence	$\nabla \cdot \mathbf{u}_{850}^f$	s^{-1}	NOGAPS
200-hPa divergence	$\nabla \cdot \mathbf{u}_{200}^f$	s^{-1}	NOGAPS
850-hPa relative vorticity	$\mathbf{k} \cdot \nabla \times \mathbf{u}_{850}^f$	s^{-1}	NOGAPS
850-hPa relative humidity	P_{0850}/P_{0850}^*	Pa Pa^{-1}	NOGAPS
500-hPa relative humidity	P_{0500}/P_{0500}^*	Pa Pa^{-1}	NOGAPS
Environmental flow	$\mathbf{u}_{850}^f, \mathbf{u}_{200}^f$	m s^{-1}	NOGAPS
SST	T_{sea}	$^{\circ}\text{C}$	TMI
Precipitation rate	r	mm h^{-1}	TMI
Current intensity	V_{\max}, p_{\min}	$\text{m s}^{-1}, \text{hPa}$	Best track
Current position	lat/lon of TC	$^{\circ}$	Best track
Translation speed	$ \mathbf{u}_{\text{TC}} $	m s^{-1}	Best track
Translation heading	$\phi = \cos^{-1}(u_{\text{TC}}/ \mathbf{u}_{\text{TC}})$	$^{\circ}$	Best track

by the parent vortex causing the TC to spin up in a fundamentally asymmetric pathway that differs from WISHE (Sang et al. 2008; Montgomery et al. 2009). Because of its dependence on small-scale deep moist convection, in this viewpoint TC intensity change is highly unpredictable, and thus ensemble and statistical methods will always be necessary (Zhang and Sippel 2009).

The detrimental effect of vertical shear on TCs is well known (Gray 1968; McBride and Zehr 1981; Merrill 1988a); however, there is some debate on the precise mechanism by which the storm weakens in shear. Since the inertial stability of the TC is weakest at upper levels, vertical shear can penetrate the storm there and ventilate its warm temperature anomaly. By hydrostatic arguments, the surface pressure must rise because of denser air at upper levels. This is consistent with high-resolution moist full-physics numerical simulation results showing a top-down weakening of TCs in shear (Frank and Ritchie 2001). DeMaria (1996) argued that another mechanism is possible. Vertical shear causes the tilting of the TC PV tower, and the resulting balanced mass and wind field associated with the PV anomalies would promote midlevel warming, and therefore tend to inhibit deep convection. The interaction of upper- and lower-level PV anomalies in vertical shear has also been studied by Flatau et al. (1994) and Jones (1995). However, recent work has also shown that TCs have an intrinsic stabilizing mechanism to external forcings such as vertical shear. Vertical shear excites discrete vortex Rossby waves, which are then damped by the differential rotation of the tangential winds, leading to symmetrization and alignment (Schechter et al. 2002; Reasor et al. 2004). This Rossby restoration mechanism is enhanced for TCs that contain vorticity skirts (Mallen et al. 2005) and for large intense TCs (Shapiro and Montgomery 1993).

When a TC moves into regions of large-scale low-level convergence, upper-level divergence, or a combination of both, its intensity may change because of an enhanced secondary circulation and associated convection. Upper-level divergence areas are commonly observed near upper-level anticyclones and downstream of upper-level troughs. When an asymmetric upper-level feature, such as a trough, interacts with a TC, it can also affect its intensity through increased vertical shear and through an eddy flux convergence of angular momentum (Black and Anthes 1971; Challa and Pfeffer 1980; Molinari and Vollaro 1989, 1990). The former process usually weakens the TC while the latter process is typically associated with intensification. The concepts of “good trough” and “bad trough” have originated through differing magnitudes of these processes. When an intense upper-level PV anomaly interacts with a TC, the shear effect may dominate the eddy flux convergence effect, while for a weaker

upper-level anomaly, the eddy flux convergence may dominate the shear effect causing intensification.

d. Compositing procedure

Using the JTWC and NHC best-track data, composites were made in a $20^\circ \times 20^\circ$ box at the initial TC position. Composites were made for four of the intensity change categories listed in Table 1: (i) weakening, (ii) neutral, (iii) intensifying, and (iv) rapidly intensifying. A rapidly weakening composite was not made because the sample size was very small. Very few storms were found to rapidly weaken over water below 30°N . However, if land interaction cases were included there exists a larger number of these cases. These composites show, on average, the large-scale environmental conditions present at $t = 0$ h, from which a given intensity change occurred in the next 24 h. Since we are primarily interested in over-water intensity changes, and because the physics of TC weakening over land is well known, the land interaction cases were discarded from the sample. It is important to note that the composites give the average conditions for a large sample of storms, and are therefore not as useful for understanding how one specific storm may change in intensity.

e. Filtering

In NOGAPS, a bogus TC vortex is inserted into the model (Goerss and Jeffries 1994; Peng et al. 2004), which is a coarse representation of the real TC. The bogus vortex is initialized in data assimilation cycle through the use of synthetic observations and the radial profile is Rankine-like and based on the observed size (Goerss and Jeffries 1994). For certain variables such as deep-layer vertical wind shear and horizontal divergence, we were interested in the large-scale environment in which the TC is embedded, without the effects of this bogus TC on that environment. A 15-day low-pass filter was applied to the NOGAPS winds in order to separate the TC from the environment for these cases. A demonstration of the removal of the TC from its environment using the low-pass filter is shown in Fig. 2. In Fig. 2a, the decomposition of the NOGAPS 850-hPa zonal wind is shown for a composite of 36 TCs in the WPAC. Here, the TC is at the center, and data is shown in a $30^\circ \times 30^\circ$ box around the TC. The right panel shows the NOGAPS analysis, the middle panel shows the field after application of the low-pass filter, and the left panel is obtained from subtracting the filtered field from the total field, and is a representation of the bogus TC winds. Note that the low-pass filtered field broadly captures the environment in which the TC is embedded, including the westerly flow to the southwest and north and easterly

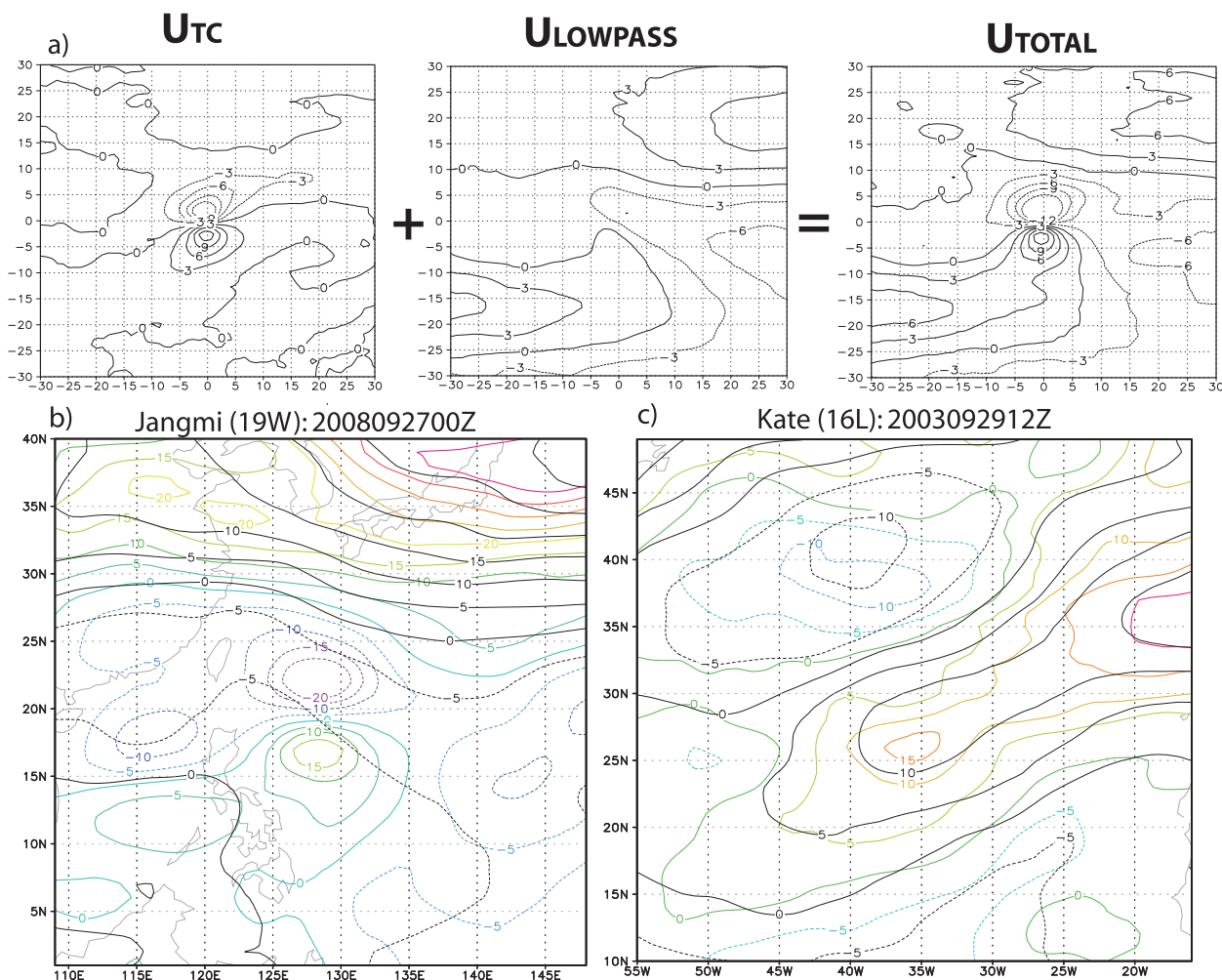


FIG. 2. The separation of NOGAPS winds into low- and high-frequency components using a 15-day low-pass filter. (a) Total, TC, and low-pass filtered 850-hPa zonal wind composite for 36 tropical cyclones in the WPAC. (b) Total zonal 500-hPa winds (color contours) overlaid with low-pass-filtered winds (black contours) for Super Typhoon Jangmi at 0000 UTC 27 Sep 2008. (c) As in (b), but for Tropical Storm Kate at 1200 UTC 29 Sep 2003.

flow to the east and southeast. To further demonstrate the effectiveness of the filter, instantaneous snapshots of the total and low-pass-filtered NOGAPS 500-hPa zonal wind are shown for Super Typhoon Jangmi (2008) and Tropical Storm Kate (2003) in Figs. 2b,c. Note that in each case the synoptic environment around the TC is largely maintained. For example, in Super Typhoon Jangmi (Fig. 2b), note that the low-pass filter removed the zonal wind dipole associated with the bogus TC vortex, but retains the easterly wind in which the TC is embedded, and the westerlies to its north.

3. Composites

In this section, the composite results for the WPAC and ATL basins are presented and discussed. The

climatology and persistence composites are presented in Figs. 3–4, and the NOGAPS and TMI data composites are presented in Figs. 5–14. For the latter composites, there are eight panels in each figure. The top four panels have the WPAC composites for each intensity change bin described in section 2b, and the bottom four panels have the ATL composites. In each group, the top-left panel is the weakening (W) composite, the top-right panel is the neutral (N) composite, the bottom-left panel is the intensifying (I) composite, and the bottom-right panel is the rapidly intensifying (RI) composite. The ordinate and abscissa are in degrees latitude and longitude, respectively, relative to the TC, which is always at the zero point. The purpose of examining the composite contour plots is to first obtain a qualitative picture of

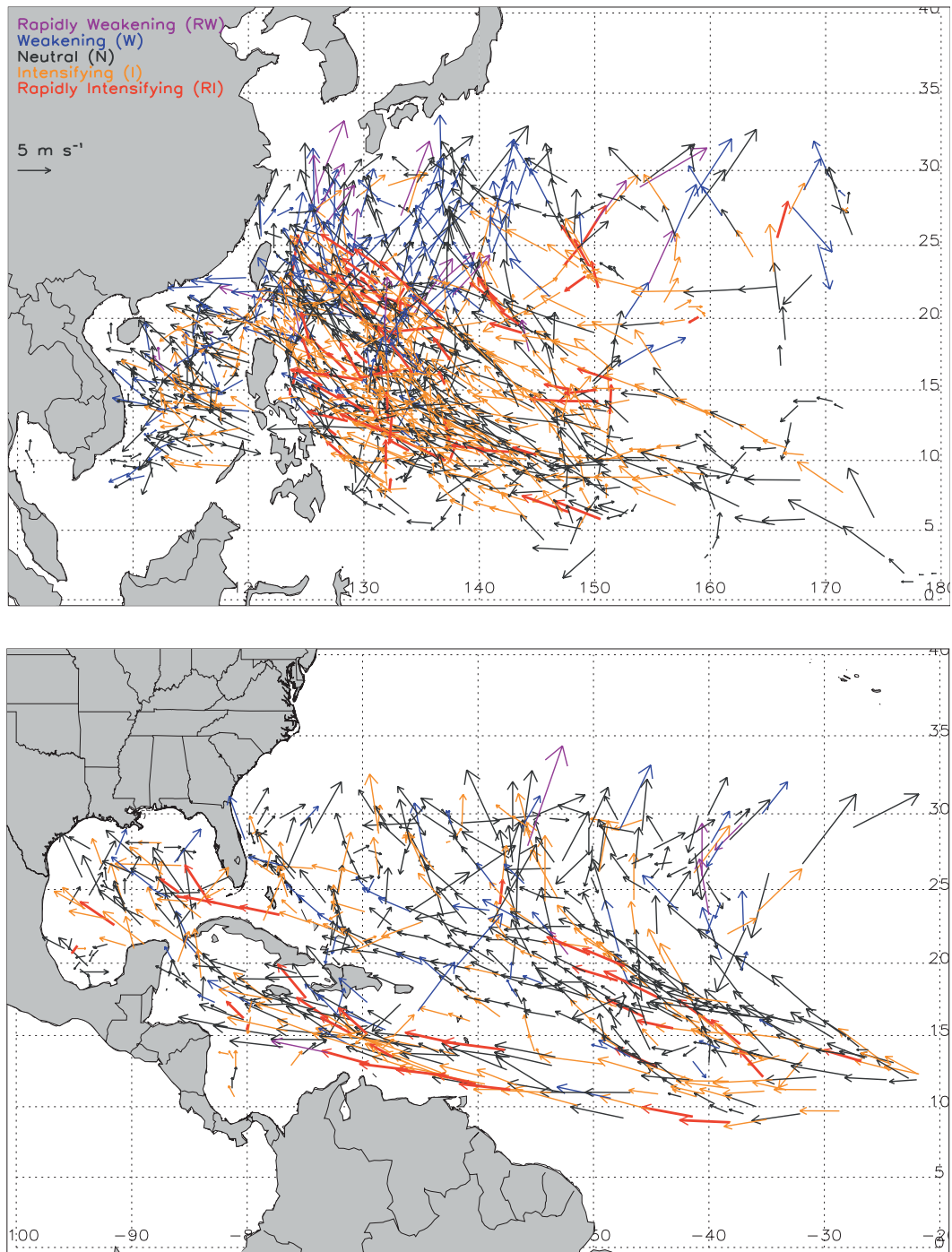


FIG. 3. The position, speed, and heading of all TCs from 2003 to 2008 undergoing intensity changes of varying magnitudes in the (top) WPAC and (bottom) ATL basins. The dataset is filtered to show only over-water changes below 30°N (from JTWC and NHC best-track datasets). Vectors for rapidly intensifying TCs are made thicker.

the environment between intensity change groups. In section 4, statistical tests are performed to obtain more quantitative results regarding the differences between RI and the other groups. Composite average values are also given in Tables 3 and 4.

a. Position, speed, and heading

The position, speed, and heading for all TCs used in this study are shown in Fig. 3. A vector is used to display these three properties: the initial position is at the base

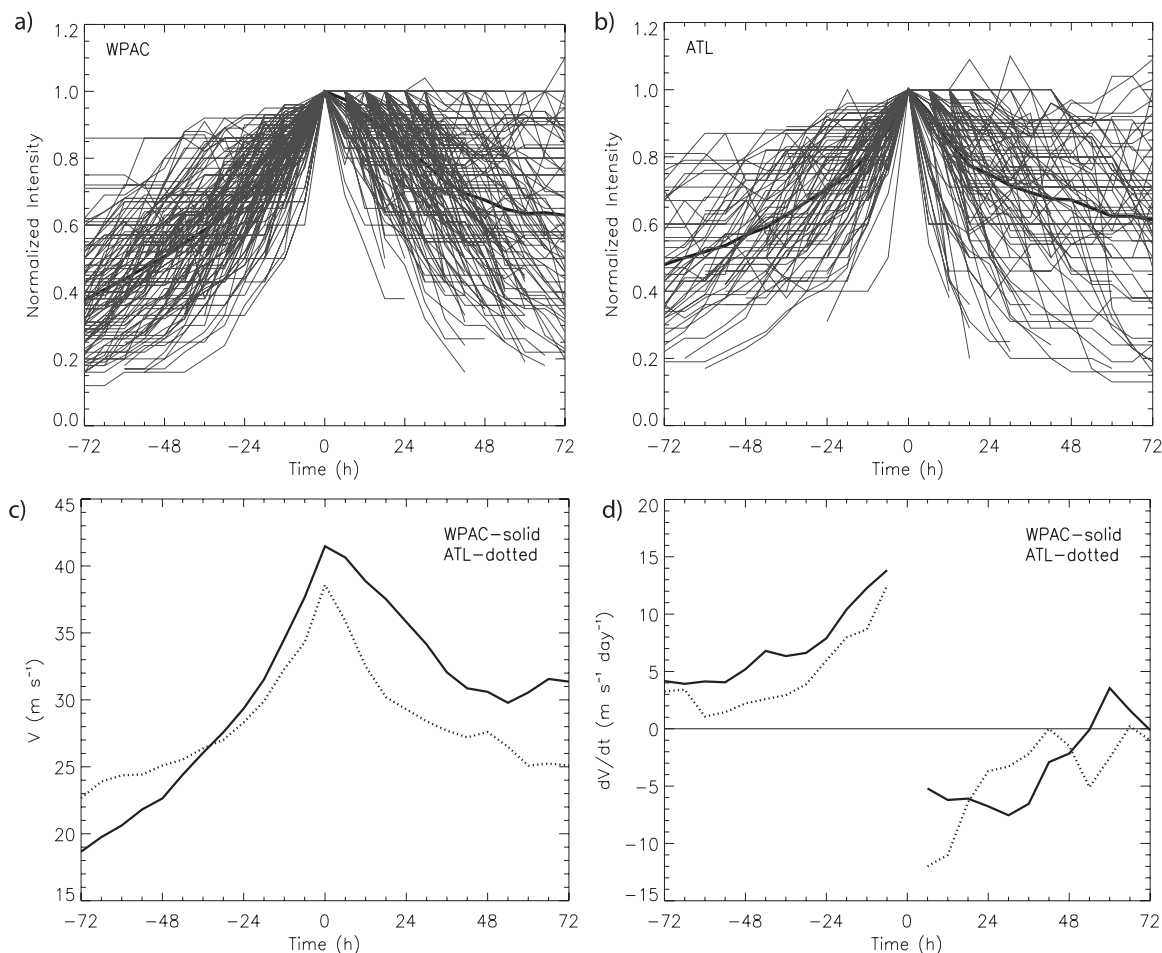


FIG. 4. Intensity life cycles in the WPAC and ATL basins using 6-h resolution JTWC and NHC best-track data for all storms from 2003 to 2008: (a) composite WPAC normalized intensity, (b) composite ATL normalized intensity, (c) composite intensity, and (d) composite intensity change (i.e., the tangent line slopes of the composite intensity curve). In (a) and (b), the solid thick curve is the average normalized intensity, and the thin gray curves are individual TCs. All plots are plotted relative to the first maximum intensity, and the normalized curves are made nondimensional by this value. In (a)–(d), time is relative to the occurrence of the first maximum intensity.

of the vector, the speed can be assessed by comparing to the reference vector, and the heading can be determined by the vector orientation. The vectors are colored based on the subsequent 24-h intensity change. The speed was calculated by using a centered second-order accurate finite-difference approximation to the position change in 12 h.

The WPAC summary is as follows. For position, it is found that (i) RI events on average happen slightly farther east than neutral or weakening events, (ii) RI events happen slightly farther north than intensifying or neutral events, (iii) neutral events occur in all portions of the basin, and (iv) weakening events occur farther north and west than the other groups. There is a hotbed for RI in the WPAC in the box (10° – 25° N, 125° – 140° E). Interestingly, in the South China Sea, there are no RI events over this time period. For speed, it is found that (Table 3) TCs in each group move at approximately the same speed. For

heading, it is found that (Fig. 2; Table 3) (i) weakening storms on average move north-northwest (344.6°), while all other storms move west-northwest to northwest (approximately 301° – 305°).

The ATL summary is as follows. For position, it is found that (i) RI events occur farther south than all other categories, and (ii) RI events happen farther west than on average than neutral or intensifying events. For speed, it is found that (Table 3) (i) RI storms move fastest (6.5 m s^{-1}), followed by intensifying, neutral, and weakening storms. For heading, it is found that (Fig. 2; Table 3) RI storms on average move west to west-northwest (288.1°), intensifying and neutral storms move west-northwest (297° – 302°), and weakening storms move northwest (320.9°).

In comparing the two basins across each intensity change bin, TCs in the ATL typically move faster and in a more westward direction than in the WPAC.

TABLE 3. Climatology and persistence average values for weakening (W), neutral (N), intensifying (I), and rapidly intensifying (RI) storms. Additionally, the differences for each quantity between RI and the other groups are shown in the last three columns, with boldface denoting statistical significance at the 95% confidence level.

Quantity	Basin	W	N	I	RI	RI - W	RI - N	RI - I
Max wind (m s^{-1})	WPAC	49.1	27.9	27.9	31.9	-17.2	4.0	4.0
	ATL	45.3	26.8	26.2	32.9	-12.4	6.1	6.7
Min pressure (hPa)	WPAC	946.5	980.4	981.8	976.7	30.2	-3.7	-5.1
	ATL	965.8	991.7	994.3	986.4	20.6	-5.3	-7.9
Avg lat ($^{\circ}\text{N}$)	WPAC	20.6	15.9	15.6	17.0	-3.6	1.1	1.4
	ATL	21.7	20.6	19.1	16.8	-4.9	-3.8	-2.3
Avg lon ($^{\circ}\text{E}$)	WPAC	129.7	134.2	136.1	136.4	6.7	2.2	0.3
	ATL	-62.2	-59.3	-60.6	-62.0	0.2	-2.7	-1.4
Avg speed (m s^{-1})	WPAC	4.7	4.6	4.9	4.6	-0.1	0.0	-0.3
	ATL	4.8	5.1	5.5	6.5	1.7	1.4	1.0
Avg heading ($^{\circ}$)	WPAC	344.6	305.1	301.6	302.7	-41.9	-2.4	1.1
	ATL	320.9	301.4	297.5	288.1	-32.8	-13.3	-9.4

b. Intensity life cycles

Before showing the various composites, it is instructive to examine the composite life cycles of TCs in both the WPAC and ATL basins. These life cycles are depicted in Fig. 4. Here the entire best-track records are used (6-h resolution), and high-latitude and land interaction cases are included.

In Figs. 4a,b, the intensity life cycles of all TCs from 2003 to 2008 are shown in the thin gray curves, and the composite mean is depicted by the thick solid curve for the WPAC and ATL basins. The intensity is normalized by the first maximum intensity. In the WPAC, on average TCs are 38% of their maximum intensity 72 h prior to maximum intensity. After reaching maximum intensity, TCs weaken at a slower rate until they are approximately 63% as intense 72 h later. There is a significant

amount of scatter between individual TCs (thin gray curves), and more scatter exists in the weakening phase. The reason for this is because the weakening phase includes three regimes: (i) weakening due to landfall, (ii) quasi-neutral behavior in a favorable environment due to the TC reaching its MPI, or (iii) weakening due to a less favorable environment or unfavorable internal dynamics, such as eyewall replacement cycles (Willoughby et al. 1982). There is also a significant amount of scatter in the intensifying phase. Some storms form and rapidly intensify to maximum intensity, while others gradually intensify to their maximum intensity. Similarly, a variety of oceanic, atmospheric and internal processes dictate the variability in these curves during this phase. In the ATL, on average TCs are 48% of their first maximum intensity 72 h prior to maximum intensity. After reaching maximum intensity,

TABLE 4. Box average values near the TC for the NOGAPS and TMI data for weakening (W), neutral (N), intensifying (I), and rapidly intensifying (RI) storms. The slope, $\partial\theta_E/\partial p$, is averaged from 1013 to 700 hPa. Additionally, the differences for each quantity between RI and the other groups are shown in the last three columns, with boldface denoting statistical significance at the 95% confidence level.

Quantity	Basin	W	N	I	RI	RI - W	RI - N	RI - I
Deep-layer shear (m s^{-1})	WPAC	12.09	10.64	9.87	10.38	-1.71	-0.26	0.51
	ATL	11.24	11.80	9.89	8.24	-3.00	-3.56	-1.65
SST ($^{\circ}\text{C}$)	WPAC	27.74	28.75	29.20	29.14	1.40	0.39	-0.06
	ATL	28.23	27.96	28.58	28.93	0.70	0.97	0.35
850-hPa relative humidity (%)	WPAC	77.83	78.75	80.01	80.19	2.36	1.44	0.18
	ATL	73.93	76.27	76.12	76.45	2.52	0.18	0.33
500-hPa relative humidity (%)	WPAC	55.56	60.65	64.25	63.46	7.90	2.81	-0.79
	ATL	48.83	50.98	52.43	53.97	5.14	2.99	1.54
850-hPa divergence (10^{-6} s^{-1})	WPAC	-1.99	-1.79	-1.95	-2.00	-0.01	-0.21	-0.05
	ATL	-1.63	-1.19	-1.40	-1.25	0.38	-0.06	0.15
200-hPa divergence (10^{-6} s^{-1})	WPAC	4.77	4.18	4.65	4.59	-0.18	0.41	-0.06
	ATL	4.61	3.02	3.37	2.84	-1.77	-0.18	-0.53
$\partial\theta_E/\partial p$ (10^3 K Pa^{-1})	WPAC	0.15	0.16	0.20	0.29	0.14	0.13	0.09
	ATL	0.35	0.28	0.32	0.31	-0.04	0.03	-0.01
850-hPa vorticity (10^{-6} s^{-1})	WPAC	14.13	13.02	13.04	14.21	0.08	1.19	1.17
	ATL	7.71	6.91	6.48	5.00	-2.71	-1.91	-1.48

TCs weaken quicker than in the WPAC. However, they end up at approximately 61% as intense 72 h afterward, similar to WPAC. There is also a good amount of scatter in the ATL in both the intensifying and weakening phases. These figures exhibit many similar characteristics to the intensity study of Emanuel (2000).

In Fig. 4c, a comparison of the actual (not normalized) intensity curves are shown for both basins. In the WPAC, on average TCs start at a lower intensity (approximately 4 m s^{-1} less) 72 h prior to the first maximum intensity than in the ATL. Additionally, they attain a peak intensity that is approximately 3 m s^{-1} greater than the ATL and they are more than 6 m s^{-1} stronger 72 h later. Figure 4d shows the derivative of the former curves, where the finite-difference approximations to the instantaneous derivatives are made by centered differences over 12 h. In both basins, TCs initially intensify at a slower rate 72 h prior to maximum intensity, and then tend to rapidly intensify approximately 24 h prior to maximum intensity. In the WPAC, TCs intensify at faster rates than in the ATL prior to the first maximum intensity. After the first maximum intensity, ATL TCs weaken more rapidly than in the WPAC. In both basins, the weakening rate becomes less with time.

In the present study, landfall and high-latitude cases were excluded. Thus, the composite life cycle for the storms considered here would exhibit less weakening than depicted in Fig. 4. On average, the ordering of the composite groups in the life cycle would be neutral or intensifying, followed by a rapid intensification episode to maximum intensity, followed by weakening. However, there is significant variability in individual TCs (Figs. 4a,b), so these intensity change episodes occur in different parts of the life cycle occasionally.

c. Initial intensity

The composite initial intensities of TCs for each intensity change bin are shown in the first two rows of Table 3. The first row shows the average maximum sustained wind and the second row shows the minimum sea level pressure from the JTWC and NHC best-track data. With regard to positive intensity changes, a similar result is found for both basins: TCs are *more* intense prior to undergoing an RI episode than an intensifying episode. This result indicates that when TCs initially form, they tend to intensify more slowly at first, until they reach a certain threshold, from which they subsequently rapidly intensify (confirmed by Fig. 4). In both basins, the TCs about to weaken were most intense. The reason for this is because the TCs are near the later part of their life cycle, farther north out of the deep tropics, and in a less favorable environment. Interestingly, in both basins there were no significant differences in the

initial intensity between intensifying and neutral storms. Both intensifying and neutral episodes tend to happen early in the TC life cycle.

Comparing the two basins, by minimum sea level pressure WPAC storms were initially deeper than ATL storms across all intensity change bins. By the maximum sustained wind, WPAC storms were initially more intense than ATL storms for the intensifying, neutral, and weakening categories, but slightly less intense for the RI category.

d. Vertical wind shear

The composite vertical wind shear is shown in Fig. 5. In the WPAC, the shear decreases moving from the weakening to the neutral to the intensifying composite. However, there is little difference between the rapidly intensifying and intensifying composites. Over the storm, the shear is between 6 and 10 m s^{-1} for these cases. In the ATL, there is not much difference between the weakening and neutral composites, however, there is less shear moving from the neutral to intensifying to rapidly intensifying composites. There is significantly less shear in the rapidly intensifying composite in comparison to the intensifying composite. Comparing both basins, it can be seen that for the intensifying and rapidly intensifying storms, the vertical shear is less in the ATL. For the neutral storms, the shear magnitudes are similar in both basins, although the phasing is different. Finally, for the weakening storms, the WPAC basin has larger shear than the ATL basin.

It is also instructive to examine the upper- and low-level wind patterns that determine the vertical shear. The low-pass-filtered winds for the WPAC and ATL at 850 and 200 hPa are shown Fig. 6. Here, only the weakening and RI composites are shown. Note that in the WPAC, in the both the weakening and RI composites, there exists a large-scale monsoon gyre (Lander 1994). The horizontal scale of this gyre is approximately 1000 km. At upper levels, the RI composite has a large-scale anticyclone, and this anticyclone is not as pronounced in the weakening composite. In the ATL, there exists an open-wave pattern in the 850-hPa filtered winds for both the RI and weakening composites. At upper levels, there is also a more pronounced anticyclone above the TC. There is an important feature in the upper-level wind vector composites for both basins: the RI composite has more easterly flow at upper levels than the weakening composite. This is a significant reason for the reduced vertical wind shear, and it is consistent with the previous ATL finding of Kaplan and DeMaria (2003). Easterly vertical wind shear may be less detrimental to a TC than westerly shear, because easterly shear tends to trap Rossby wave energy in the lower troposphere (Wang and Xie 1996).

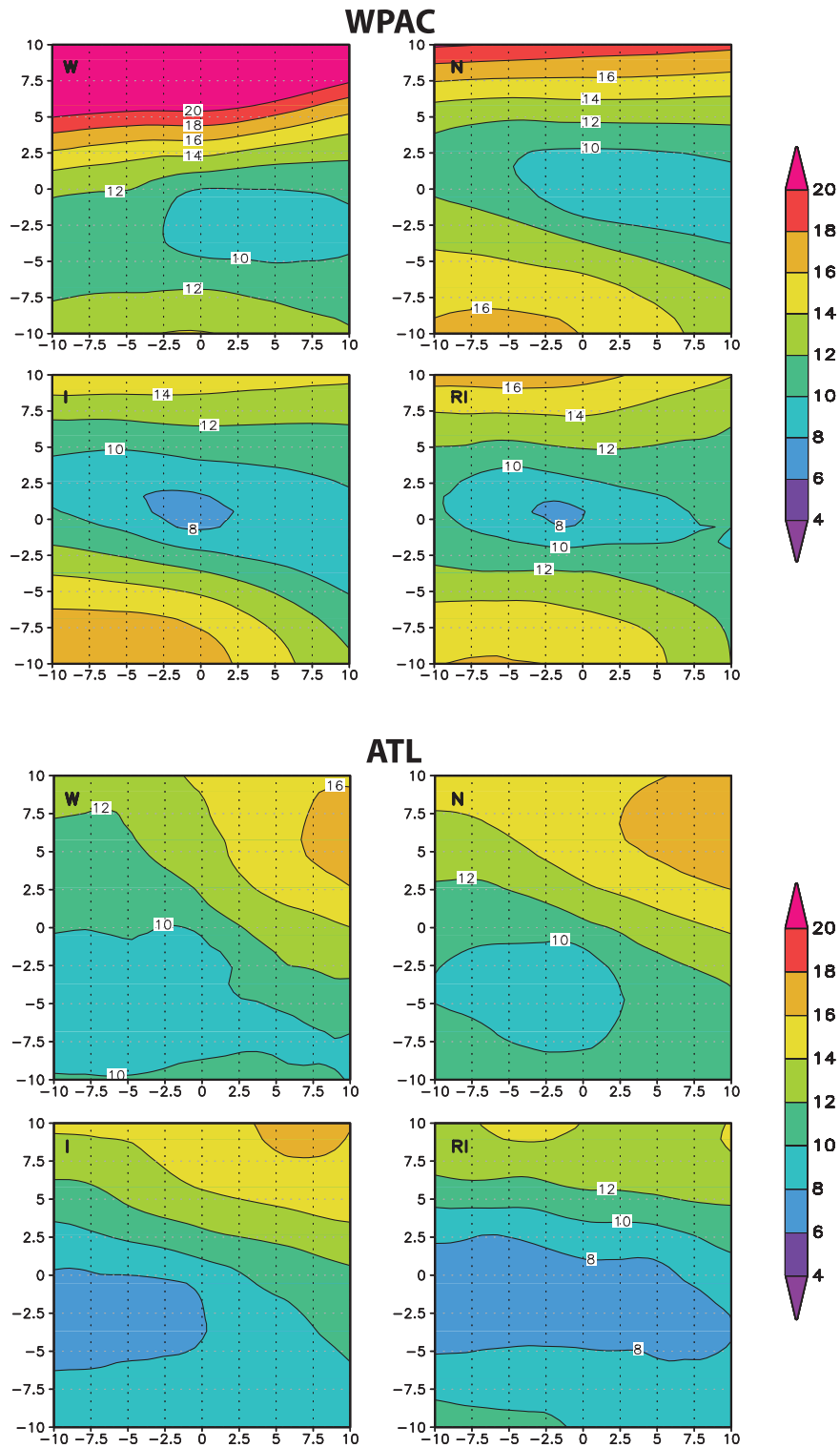


FIG. 5. Composite magnitude of the NOGAPS deep-layer wind shear vector, $|\mathbf{u}_{200}^f - \mathbf{u}_{850}^f|$ (m s^{-1}), for the (top) WPAC and (bottom) ATL basins.

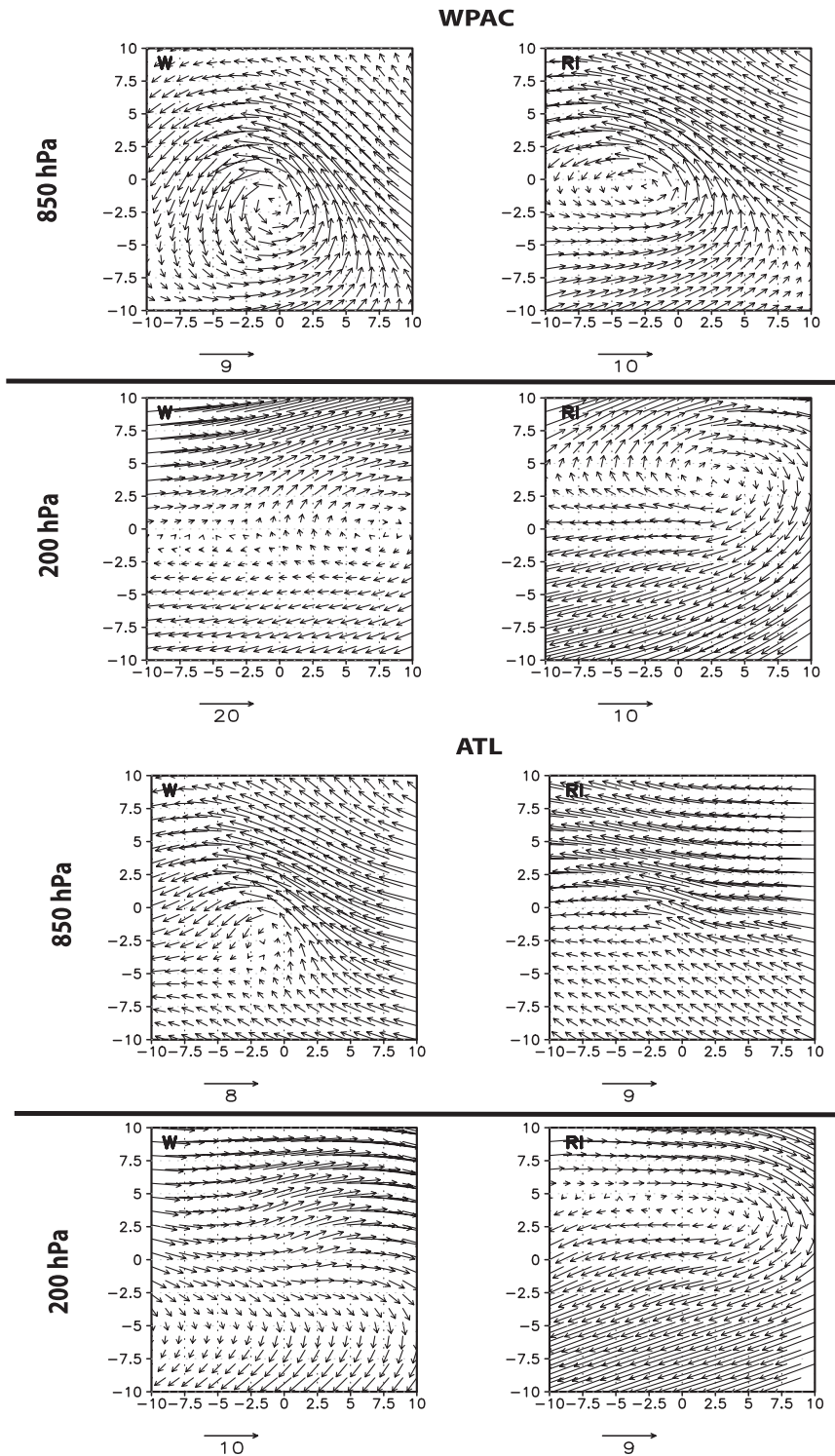


FIG. 6. Filtered wind vectors at lower (850 hPa) and upper levels (200 hPa) for (top) the WPAC and (bottom) ATL basins. The reference vector has units of m s^{-1} .

e. Sea surface temperature

Before examining the composite SST field for each intensity change group, it is instructive to first view the large-scale climatology for each basin. The climatological mean SST for July–October 2003–08 are shown in Fig. 7. In the WPAC, there is a very large area of SSTs greater than 29°C. In the ATL, this area is smaller and confined primarily to the Gulf of Mexico, Caribbean Sea, and east of the Lesser Antilles. In the WPAC, SSTs vary significantly meridionally (particularly at higher latitudes), but only weakly zonally. By contrast, there exists a strong zonal variance in the ATL SSTs, with temperatures cooling toward the east. This position dependence of SST will be revealed in the composite plots for individual categories of TC intensity change.

The composite SST contour plots are shown in Fig. 8 and the $10^\circ \times 10^\circ$ box average values are listed in Table 4. In the WPAC, the SSTs are much cooler for weakening storms (27.74°C) than all other categories. There also exists a strong north–south gradient, with SSTs ranging from 26° to 29°C. The SSTs warm significantly progressing to the neutral group (28.75°C). The SSTs for intensifying and RI TCs are slightly warmer than for neutral TCs. Interestingly, the SSTs are similar between intensifying and RI (29.20° and 29.14°C, respectively) storms. In the ATL, there is a natural progression of warming SSTs moving from weakening to RI storms. Similar to the WPAC, there is not much difference between the SSTs at $t = 0$ h for intensifying and RI storms (28.58° and 28.93°C, respectively). Comparing both basins, we see that SSTs in the WPAC are warmer than SSTs in the ATL for all categories except weakening. The reason the weakening SST composite is cooler in the WPAC than the ATL is due to the fact the most storms in the WPAC weaken when entering more northern latitudes (see top panel of Fig. 3). In the ATL, on the other hand, weakening events happen over a broader range of latitudes (bottom panel of Fig. 3).

f. Instability

The composite instability for each intensity change group is shown in Fig. 9. Here, the area-averaged equivalent potential temperature in a $10^\circ \times 10^\circ$ box is shown as a function of pressure. The average slope in the lower troposphere $\partial\theta_E/\partial p$ measures the level of conditional instability in the local vicinity of the TC. Larger instability would tend to promote more vigorous deep convection and vortex intensification.

In the WPAC (top panel of Fig. 9), note that there is a progression to a more conditionally unstable troposphere moving from the weakening to the RI composite.

The largest instability is for RI storms, intensifying and neutral storms have similar instability, and weakening storms are more stable. The average slope for each group below 700 hPa is shown in Table 4. Note that for RI storms, $\partial\theta_E/\partial p \approx 0.29 \times 10^3 \text{ K Pa}^{-1}$. In the ATL, RI, intensifying and neutral storms all have a similar level of conditional instability. In comparing both basins (Table 4), note that the ATL is on average more unstable than the WPAC across all intensity change groups. These results show that instability is a differentiating factor between intensifying and RI storms in the WPAC, but not in the ATL.

g. Low-level relative humidity

The low-level relative humidity for the each intensity change group is shown in Fig. 10. Here, the composites are made in a $40^\circ \times 40^\circ$ box to illustrate more of the synoptic-scale environment in which the TC is embedded.

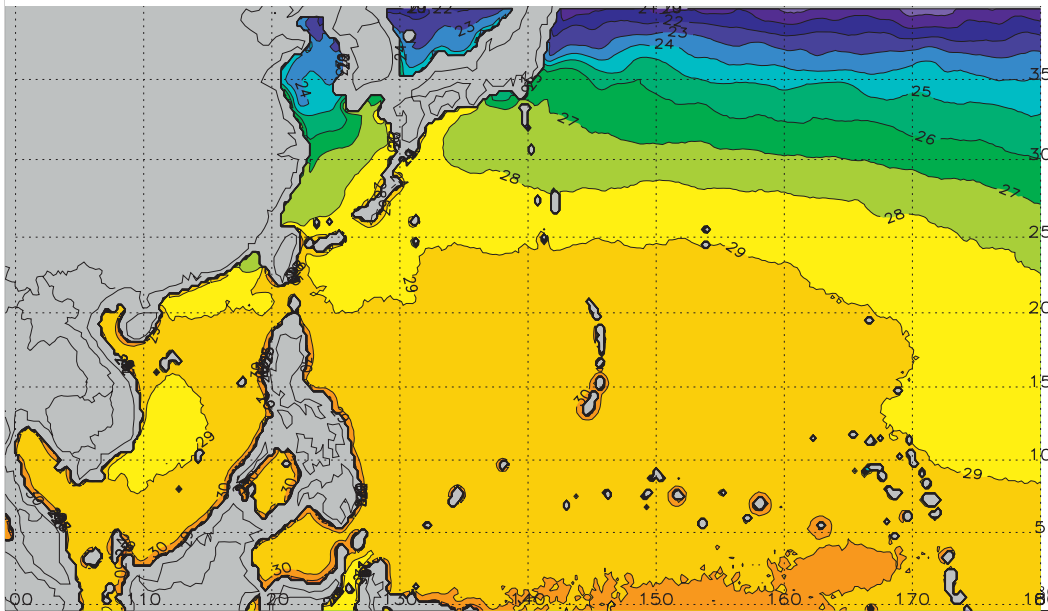
In the WPAC, in the weakening composite there is drier air (approximately 65%–68% RH) wrapping into the storm on the northwest periphery. Moving to the neutral composite, this dry air is no longer existent, and relative humidities near the TC core are approximately 77%–80%. The intensifying and RI composites are quite similar to the neutral composite in terms of spatial structure, but slightly more humid (80%–83%). The weakening composite has the largest core relative humidity because on average the storms are more intense, and thus have larger moisture convergence. In the ATL, a similar picture exists. In the weakening composite, there is drier air evident on the western portion of the storm, which is not as pronounced as in the other composites. In the ATL, the RI composite has slightly more humid air around the TC than the intensifying or neutral composites.

Examining Table 4, which depicts the average humidity in a $20^\circ \times 20^\circ$ box, we see that there is little difference in low-level relative humidity for the RI, intensifying and neutral composites in the ATL, and little difference in the humidity for RI and intensifying TCs in the WPAC. In both basins, the weakening composite is notably drier than the RI composite (on average 2.5% less relative humidity). Also note that the WPAC is significantly moister than the ATL at low levels (approximately 3%–4%). This is likely due to enhanced moisture convergence from the monsoon trough and gyre that exists there.

h. Midlevel relative humidity

The midlevel relative humidity for the each intensity change group is shown in Fig. 11. Here, as well, the composites are made in a $40^\circ \times 40^\circ$ box centered at the TC location. In both basins, there is natural progression

WPAC



ATL

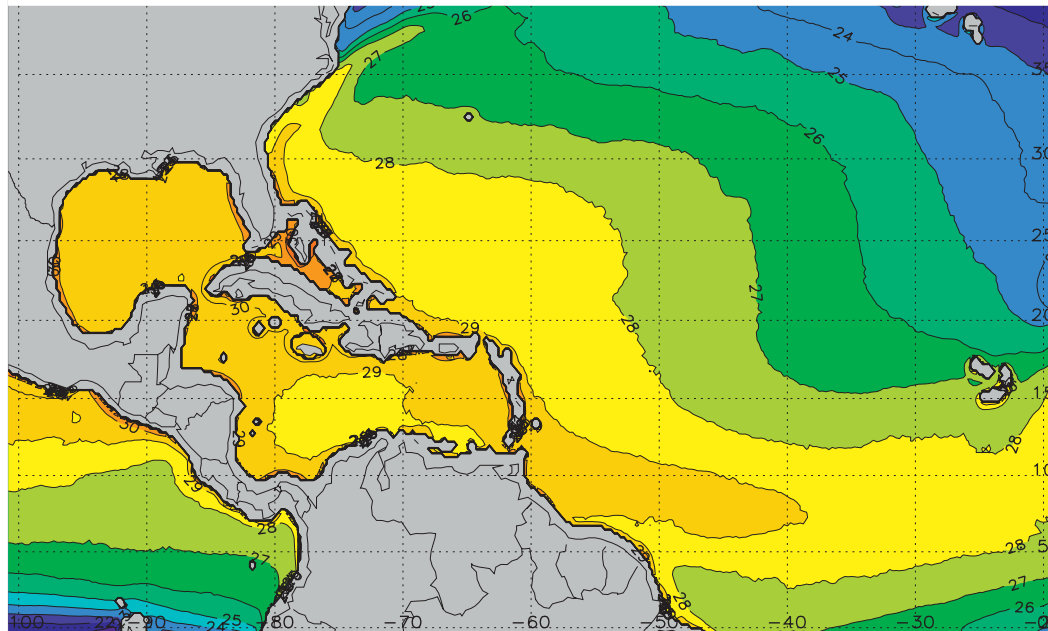


FIG. 7. July–October climatological mean TMI sea surface temperatures ($^{\circ}\text{C}$) for 2003–08 for WPAC and ATL basins.

of the environment becoming moister moving from the weakening to the RI composites.

In the WPAC, note that drier air (36%–40%) is wrapping into the storm in the weakening composite. Moving to the neutral composite, there exists drier air to the

north, but it is not wrapping into the storm as much. The intensifying composite is similar to the neutral composite. The RI composite is slightly moister than both the intensifying and neutral composites, particularly south of the TC, with peak values near 76%–80%.

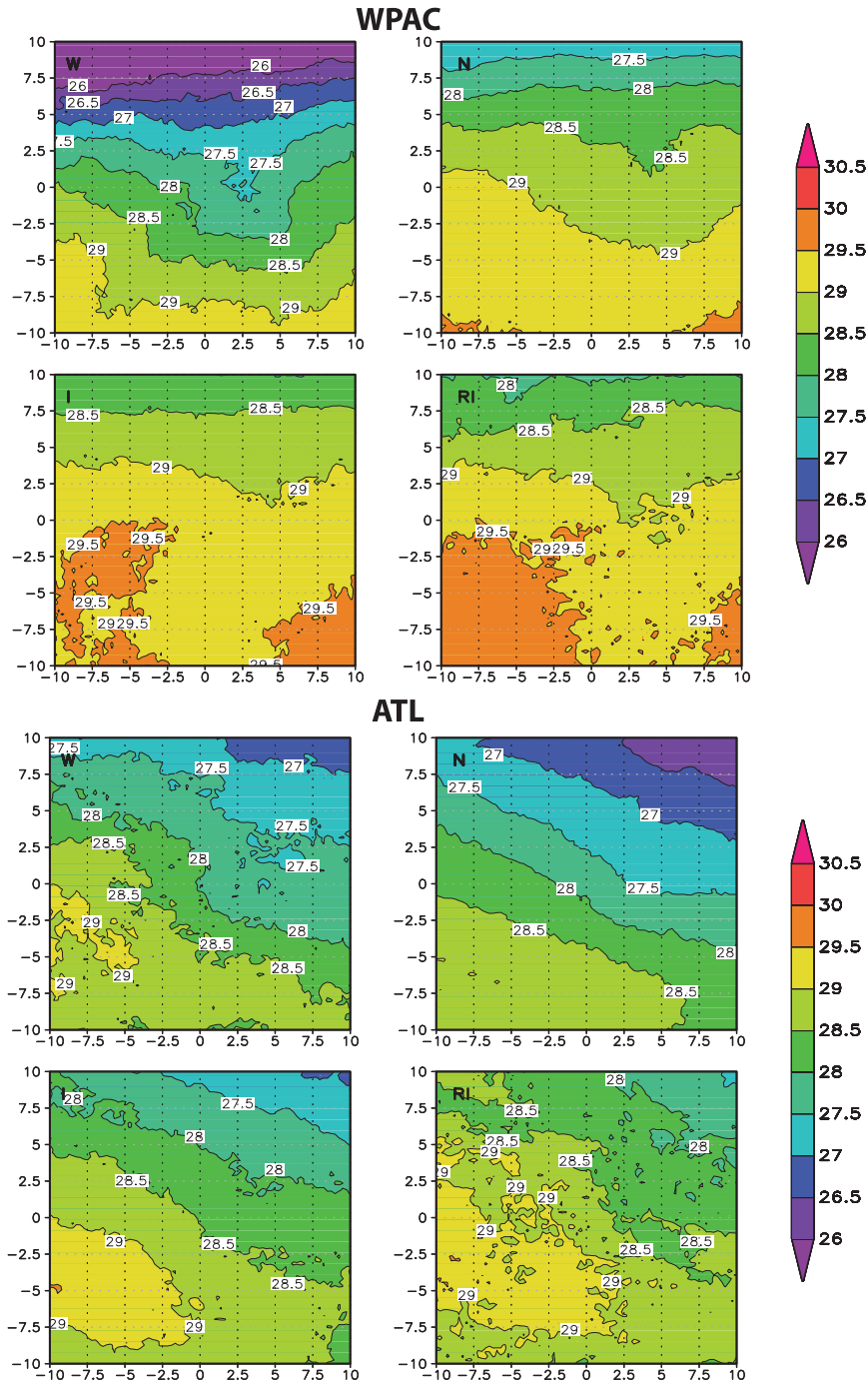


FIG. 8. As in Fig. 5, but for TMI sea surface temperature: T_{sea} ($^{\circ}\text{C}$).

In the ATL, again, a similar picture exists. Even drier air than in the WPAC (32%–36%) is clearly wrapping into the TC on the western side in the weakening composite. Progressing to the other categories, this drier air is less pronounced there. Again, the RI composite is most moist, with a large area of relative humidity of approximately 64%–68% south of the TC.

Interestingly, the RI composite in the ATL exhibits very dry air (32%–36%) just north of the TC. This is anecdotal evidence that TCs can rapidly intensify with very dry air in their vicinity, as long as that air is not entering the cyclone.

In comparing both basins, there are stark differences. The WPAC is significantly more moist at midlevels than

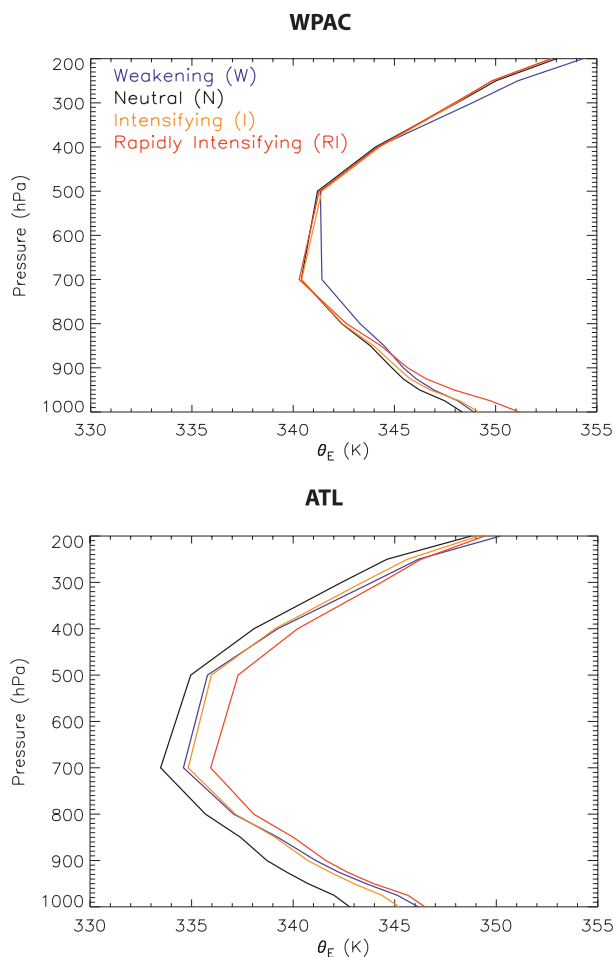


FIG. 9. Average NOGAPS $\theta_E(p)$ in a 10° box around the TC for each intensity change bin: (top) WPAC and (bottom) ATL.

the ATL across all intensity change bins (on average approximately 10% higher).

i. Upper- and low-level divergence

The low- and upper-level divergence are analyzed at 850 and 200 hPa, respectively, and the results are shown in Figs. 12–13. In the WPAC, note that there exists low-level convergence in the entire $20^\circ \times 20^\circ$ box for all intensity change categories, and there are no significant differences in magnitude or scale. This is due to the fact that the majority of the storms are located within the monsoon gyre and trough. In the ATL, the low-level convergence is weaker, and in each intensity change group there exists some low-level divergence north of the TC. Interestingly, this divergence is slightly more pronounced in the RI composite than the other groups. In comparing the intensity change groups, we see that the RI composite has the largest low-level convergence south of the TC. In comparing the two basins, the

WPAC has a larger areal extent and magnitude of low-level convergence (see also Table 4).

Moving to the upper-level divergence (Fig. 13), in the WPAC the weakening composite has the largest upper-level divergence, while the upper-level divergence in the neutral, intensifying and rapidly intensifying groups are similar. A similar picture exists in the ATL; however, the RI group appears to have smaller upper-level divergence than the other groups. As shown in the next section, however, this result is not statistically significant. The largest upper-level divergence in the weakening composite can be most likely attributed to two factors: (i) weakening TCs often are interacting with upper-level troughs, and (ii) weakening TCs are on average significantly more intense than the other groups (Table 3). Since the upper-level circulation of TCs is very large (Elsberry et al. 1987), a portion of the divergence in Fig. 13 is induced by the upper-level outflow from the TC. In comparing both basins, the WPAC has a larger magnitude and areal extent of the upper-level divergence than the ATL, similar to what was observed in the low-level convergence.

j. Background relative vorticity

The low-level background relative vorticity is shown in Fig. 14 for each intensity change group. Note that this vorticity is calculated using the low-pass-filtered winds, and therefore the bogus TC vorticity is nonexistent in these plots. It can be easily seen that in each basin, there are not significant differences between the intensity change bins. There exists an ample supply of relative vorticity in each bin near the TC center. Typically there is a region of anticyclonic relative vorticity to the north of the TC. In comparing the two basins, the WPAC has a larger magnitude and areal extent of its relative vorticity pool in comparison to the ATL (see also Table 4). In the ATL, the relative vorticity is mostly produced by the meridional gradient of the zonal wind, while in the WPAC there is also a significant contribution from the zonal gradient of the meridional wind.

k. Rain rate

The TMI rain-rate data was examined for each group to assess the differences in precipitation for each intensity change group. The rain rate was found to be a function of the current TC intensity, and not the subsequent 24-h intensity change. The correlation of rain rates with TC intensity has also been emphasized by Cecil and Zipser (1999) and Hoshino and Nakazawa (2007). As such, in both basins the weakening composite had the largest rain rates, followed by the RI composite, while the intensifying and

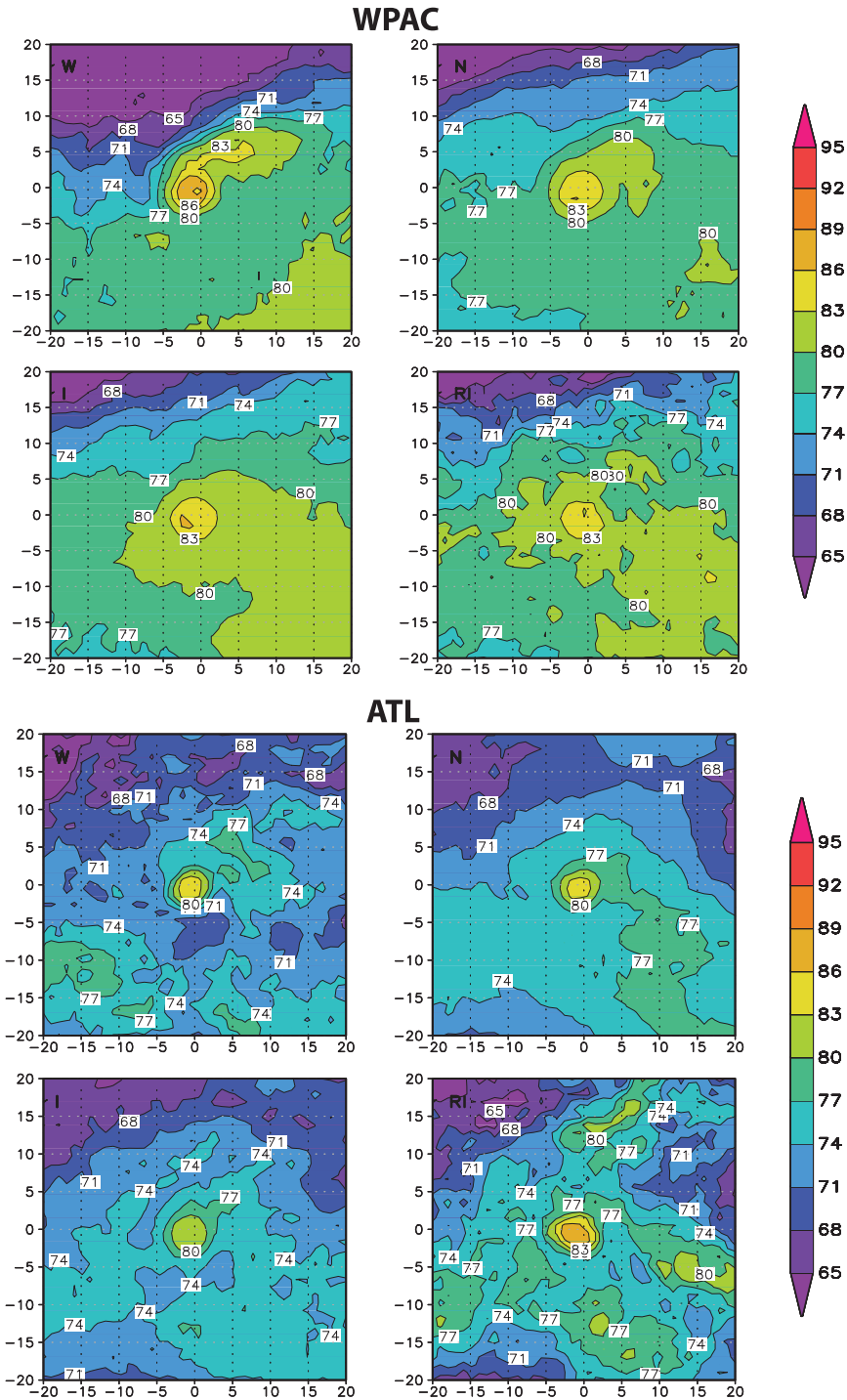


FIG. 10. As in Fig. 5, but for NOGAPS 850-hPa relative humidity: $100 \times p_{v850}/p_{v850}^*$ (Pa Pa^{-1}).

neutral composites had similar rain rates. Contrasting the two basins, in the WPAC rain rates were approximately 25%–50% higher across all intensity change groups than in the ATL, and the TC precipitation shield was approximately twice as large in horizontal

scale. Larger precipitation shields have also been found in the WPAC in the studies of Lonfat et al. (2004) and Wingo and Cecil (2010). As an example of the differences in rain rates between the two basins, Fig. 15 shows the TMI rain rates for neutral TCs in the

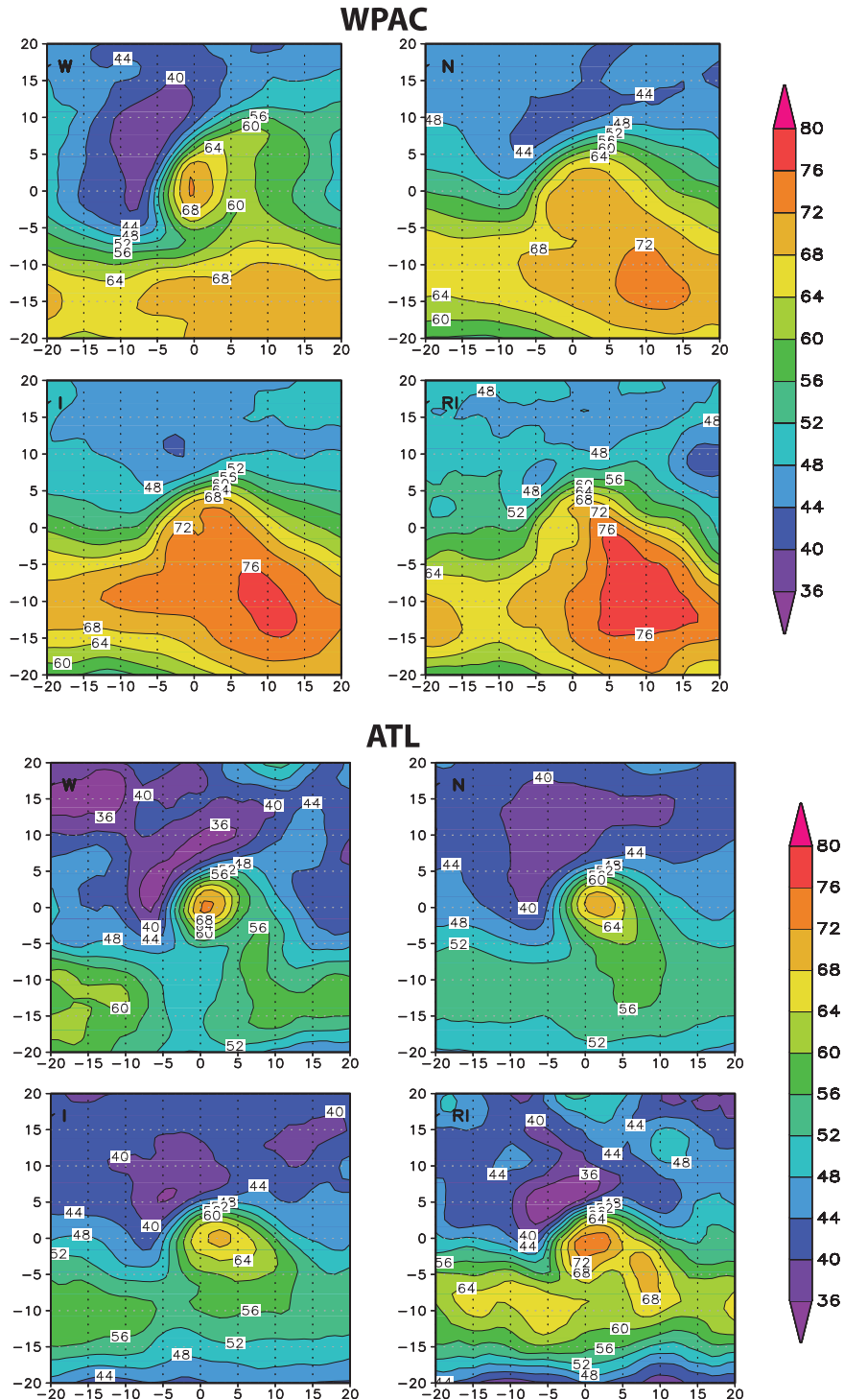
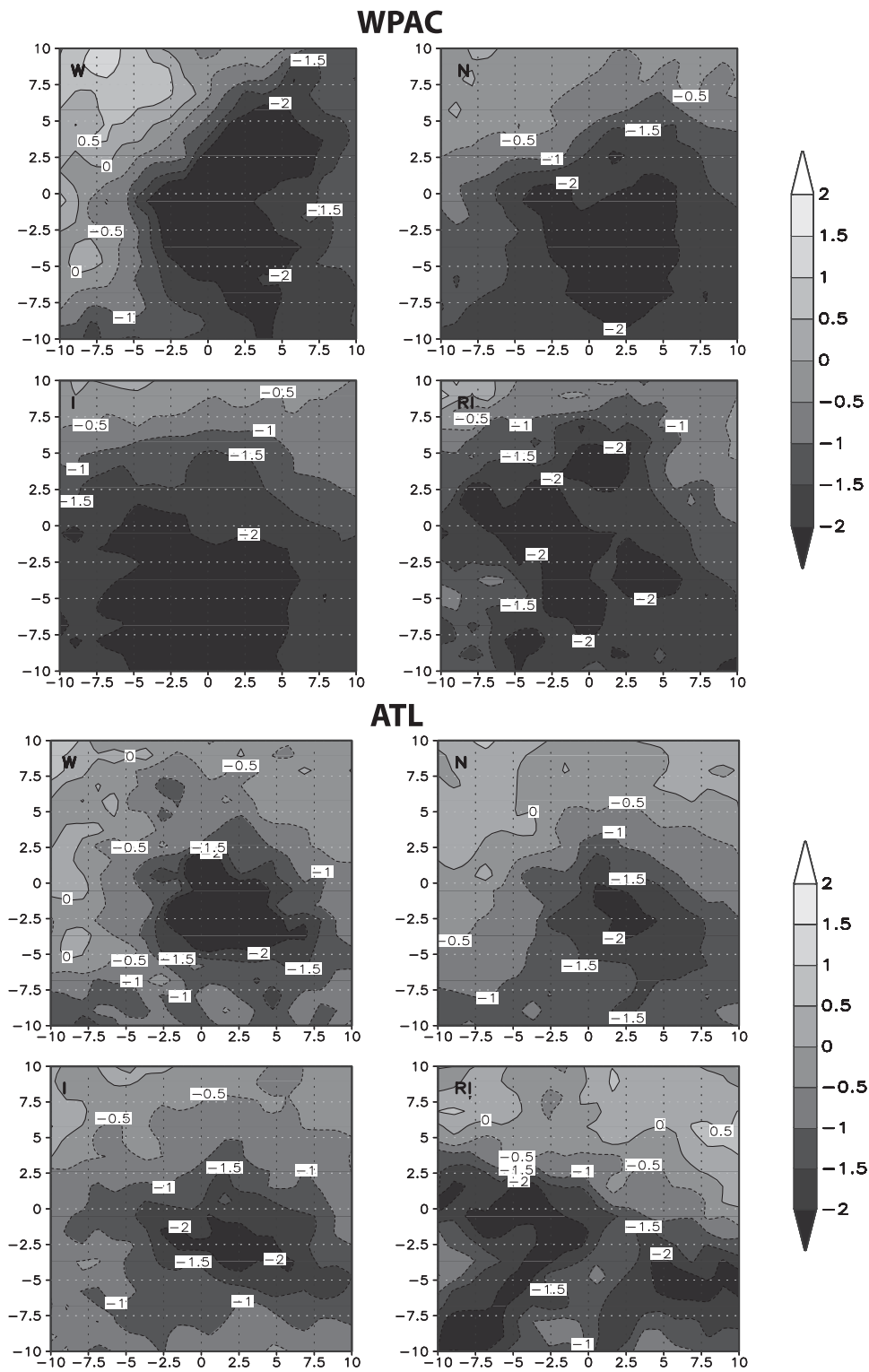


FIG. 11. As in Fig. 5, but for NOGAPS 500-hPa relative humidity: $100 \times p_{v500}/p_{v500}^*$ (Pa Pa^{-1}).

WPAC and ATL basins. Note that WPAC precipitation shield (as measured by the diameter of the 0.6 mm h^{-1} contour) is twice as large, and peak rain rates are over 1.8 mm h^{-1} in the WPAC, while peak rain rates are

1.2 mm h^{-1} in the ATL. This is not surprising since the composites indicated significant moister air at low and mid levels in the WPAC, as well as a larger and stronger area of low-level convergence.



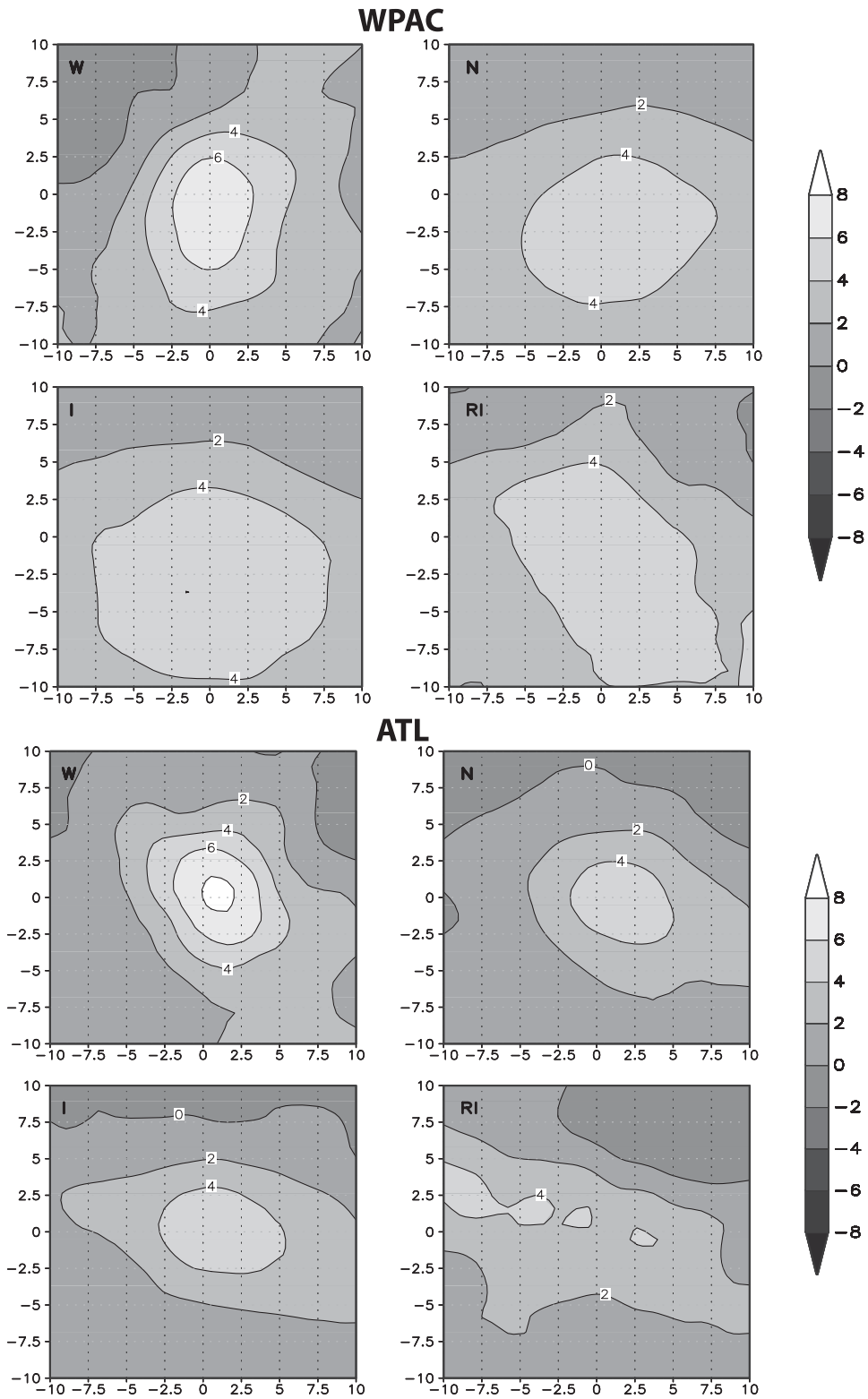


FIG. 13. As in Fig. 5, but for NOGAPS 200-hPa divergence: $\nabla \cdot \mathbf{u}_{200}^f$ (10^{-6} s^{-1}).

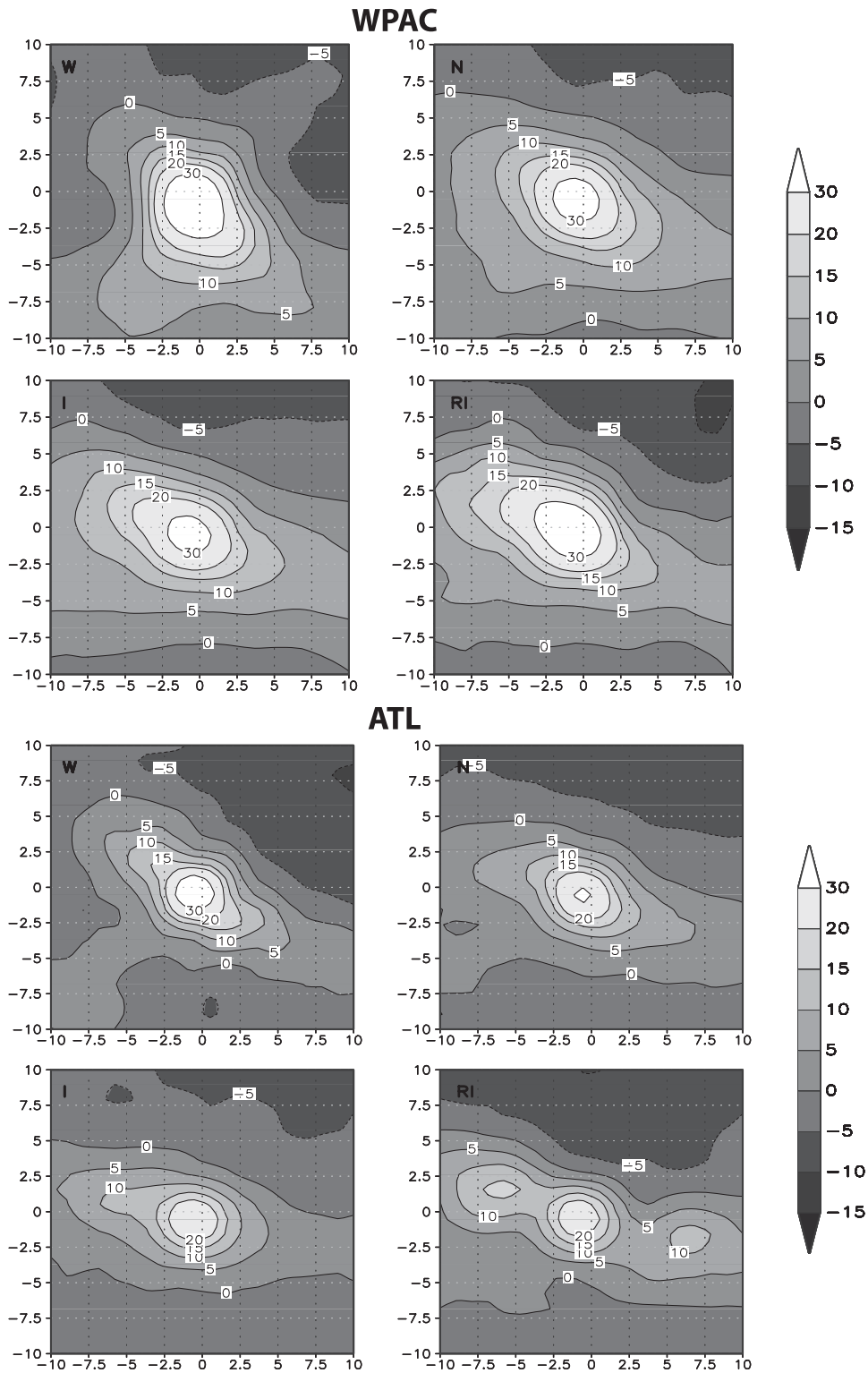


FIG. 14. As in Fig. 5, but for NOGAPS 850-hPa filtered relative vorticity: $\mathbf{k} \cdot \mathbf{V} \times \mathbf{u}_{850}^f$ (10^{-6} s^{-1}).

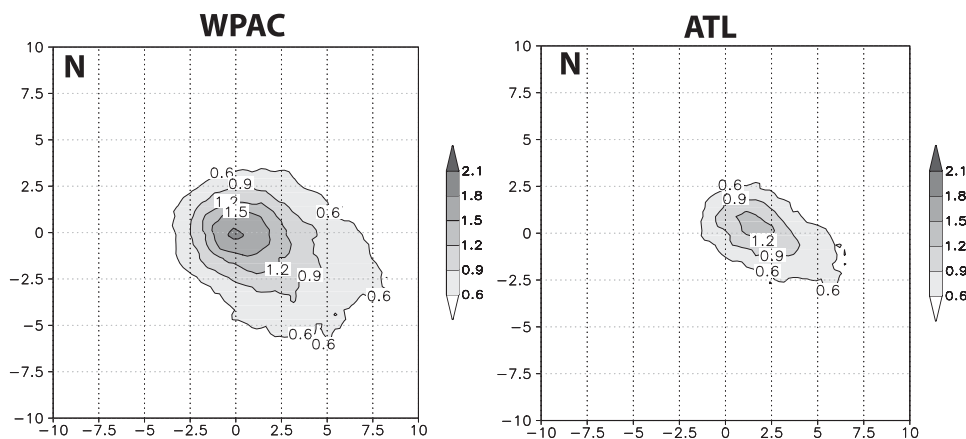


FIG. 15. TMI instantaneous rain rates in mm h^{-1} for neutral TCs in the WPAC and ATL basins.

1. TC outflow

In the environmental compositing study of Merrill (1988b), a significant difference in the outflow pattern was found between intensifying and nonintensifying TCs. For intensifying TCs, the upper-level outflow exhibited open streamlines while for nonintensifying TCs closed streamlines existed. The existence of open streamlines allows the TC to ventilate itself with the surrounding environmental flow. A similar result was confirmed in this compositing study by examining the unfiltered upper-level winds. The RI composite exhibited strong upper-level ridging to its east with more open streamlines than the neutral (nonintensifying) composite.

4. Synthesis

In the previous section, composites of the environment near TCs undergoing intensity changes of varying magnitudes were examined. In this section, statistical tests are performed in order to quantify whether or not there exists statistically significant differences between the rapidly intensifying TCs and the other groups. The purpose of these tests to better understand differences in the environment for those TCs that rapidly intensify and TCs the intensify more slowly, stay at approximately the same intensity, or weaken. A two-tailed t test was performed for all data under the null hypothesis that there is no difference between RI storms and others (i.e., $\text{RI} - \text{W} = 0$, $\text{RI} - \text{N} = 0$, and $\text{RI} - \text{I} = 0$). The criterion to *reject or fail to reject* this null hypothesis was determined using a p value of 0.05, and 95% confidence limits were enforced. Since our data is limited, the statistical test takes into account the variability in each environmental and climatology and persistence parameter in order to estimate the likelihood that the null hypothesis would hold true for an infinite sample of TCs. In sections 4a and

4b, a difference is only noted if it was statistically significant at the 95% confidence level. When similarities are stated, it signifies that there was a failure to reject the null hypothesis.

a. Climatology and persistence data

The differences in the climatology and persistence data are summarized in the last three columns of Table 3. Boldface type in these columns signifies that the null hypothesis was rejected, or that the difference shown is statistically significant at the 95% confidence level. The differences between RI and weakening TCs for both basins are as follows: (i) RI storms are initially weaker (by maximum sustained wind, -17.2 m s^{-1} in the WPAC and -12.4 m s^{-1} in the ATL), (ii) farther south, and (iii) have a more westward motion. In the WPAC, RI events happen farther east ($+6.7^\circ$ on average), while in the ATL the average longitude is similar. In the ATL, RI storms move significantly faster ($+1.7 \text{ m s}^{-1}$), while in the WPAC, RI and weakening TCs have similar speeds. The RI storms are more intense than neutral storms in both basins. As discussed in section 3b, this occurs because TCs typically have an RI episode later in their life cycle. In the WPAC, there are no statistically significant differences between RI and neutral TCs in average latitude, longitude, speed, and heading. In the ATL, RI storms are farther south than neutral storms, move faster, and have a more westward component to the heading. Finally, the comparison of the RI and intensifying group is as follows. The RI storms are initially more intense than intensifying storms in both basins. Similar to RI-N comparison, there are no statistically significant differences with respect to average latitude, longitude, speed, and heading in the WPAC. In the ATL, RI storms are farther south than intensifying storms, move faster ($+1.0 \text{ m s}^{-1}$), and have a more westward component to the heading.

Synthesizing the results, there are many differences in the climatological and persistence variables between RI and weakening TCs in both basins. In the ATL, there are also many differences between RI and neutral-intensifying TCs, while in the WPAC, the only difference is that the initial intensity for RI storms is larger.

b. Environmental data

The environmental data are summarized in Table 4. Here, $10^\circ \times 10^\circ$ box average values about the TC are listed for all variables except the relative humidity, which are averages of a $20^\circ \times 20^\circ$ box. The reason that a larger box was used for relative humidity was to minimize the effects of the TC vortex moisture and capture more of the environment. There are many differences in the environment between RI and weakening TCs in both ocean basins, as expected. The RI storms have weaker deep-layer vertical wind shear (more pronounced in the ATL), warmer SSTs (more pronounced in the WPAC), and larger low- and midlevel moisture content. In the ATL, RI storms have larger low-level relative humidity and smaller upper-level divergence, while the low-level convergence, instability, and low-level vorticity are similar. In the WPAC, RI storms have significantly larger instability, while the low-level humidity, low- and upper-level divergence, and low-level relative vorticity are similar. Moving to the comparison of the RI and neutral groups, the main differences are that in both basins RI storms have slightly warmer SSTs and more midlevel moisture than neutral storms. In the ATL, the SSTs are 0.97°C warmer, while in the WPAC the SSTs are 0.39°C warmer. Both basins have similar low-level vorticity and low- and upper-level divergence. In the WPAC, RI storms have a larger instability while the vertical wind shear is similar. In the ATL, RI events happen in weaker wind shear, while the instability is similar. Finally, moving to the comparison between RI and intensifying groups, very few statistically significant differences are found in the environmental parameters. In the WPAC, the instability is larger, while the vertical shear is similar. In the ATL, the vertical shear is weaker, while the instability is similar. The low- and midlevel relative humidity, low-level vorticity, and low- and upper-level divergence are similar. In both basins, there are no statistically significant differences in SST between RI and intensifying TCs, indicating that the rate at which TCs intensify is not critically dependent on SST. However, given that Kaplan et al. (2010) found that RI storms had significantly larger ocean heat content than TCs that did not rapidly intensify, in future work it would be interesting to see if there is a statistically significant difference in ocean heat content between RI and intensifying TCs.

The average values were also tabulated using a $6^\circ \times 6^\circ$ box around the TC center, and the results are presented in Table 5. The reason for showing smaller box average values is that an argument may be made that the TC may be affected by the environment in a smaller area, closer to the actual size of the TC. Broadly, these results are consistent with the $10^\circ \times 10^\circ$ box results in terms of comparing the different intensity change groups. The magnitudes of the values are slightly different, however. For example, the vertical wind shear magnitudes are decreased in all groups. The RI value for the ATL is now closer to the findings of Kaplan and DeMaria (2003). Note that the relative humidity averages were not shown for the smaller box because they would only capture the moisture of the TC, which is largely a function of the current TC intensity, and not the surrounding environment.

Synthesizing the results, the environment became progressively more favorable moving from the weakening to the intensifying group. However, there were few environmental differences between the RI and intensifying groups.

c. Comparison to other RI studies

It is important to distinguish the findings from this study from other work on environmental characteristics of rapidly intensifying TCs: Kaplan and DeMaria (2003) and most recently, Kaplan et al. (2010, hereafter KDK). KDK developed an updated RI index based upon examination of large-scale environmental and oceanic conditions and climatology and persistence variables for the North Atlantic and eastern North Pacific basins. We now discuss similarities and differences between the methodologies and results from that study and the present work for the ATL basin.

For the environmental data, KDK uses the National Centers for Environmental Prediction (NCEP) operational analysis data at $2^\circ \times 2^\circ$ resolution. This in contrast to our work, which uses the $1^\circ \times 1^\circ$ operational analysis of NOGAPS. Second, KDK presents environmental parameter results in terms of averages in a radius from the TC center (e.g., $r = 0\text{--}500$ km for deep-layer shear or $r = 0\text{--}1000$ km for upper-level divergence). We, on the other hand, present results as $10^\circ \times 10^\circ$ and $6^\circ \times 6^\circ$ box averages about the TC center. By matching areal regions using estimates of $111 \text{ km } ^\circ\text{latitude}^{-1}$ and $104 \text{ km } ^\circ\text{longitude}^{-1}$, the former value corresponds to $r = 0\text{--}606$ km, and the latter value corresponds to $r = 0\text{--}363$ km. Third, KDK uses unfiltered winds for deep-layer shear and upper-level divergence (with the TC vortex removed), and average the values from $t = 0\text{--}24$ h along the TC track. We use low-pass-filtered winds, and show results at $t = 0$ h. Finally, we separate our data by four different bins of the TC intensification

TABLE 5. The $6^\circ \times 6^\circ$ box averages values near TC for the NOGAPS and TMI data for weakening (W), neutral (N), intensifying (I), and rapidly intensifying (RI) storms. The slope, $\partial\theta_E/\partial p$, is averaged from 1013 to 700 hPa.

Quantity	Basin	W	N	I	RI
Deep-layer shear (m s^{-1})	WPAC	10.90	9.53	8.73	9.32
	ATL	10.84	11.46	9.37	7.75
SST ($^\circ\text{C}$)	WPAC	27.68	28.76	29.26	28.90
	ATL	28.20	27.93	28.57	28.95
850-hPa divergence (10^{-6} s^{-1})	WPAC	-2.50	-1.98	-1.98	-2.09
	ATL	-2.12	-1.46	-1.65	-1.41
200-hPa divergence (10^{-6} s^{-1})	WPAC	6.23	4.77	5.08	5.24
	ATL	6.46	4.07	4.54	3.50
$\partial\theta_E/\partial p$ (10^3 K Pa^{-1})	WPAC	0.01	0.10	0.14	0.23
	ATL	0.20	0.21	0.24	0.21
850-hPa vorticity (10^{-6} s^{-1})	WPAC	25.12	21.59	21.03	24.14
	ATL	16.71	14.38	13.01	10.71

rate, from weakening to rapidly intensifying. KDK and Kaplan and DeMaria (2003) use two groups: rapidly intensifying (RI) and all the rest (non RI).

To make a comparison with KDK, we also made a composite of each environmental parameter for non-RI cases, which includes the weakening, neutral, and intensifying categories discussed earlier. This non-RI group was found to most closely match our neutral group. A primary difference between KDK and the present study is their finding of stronger upper-level divergence for RI cases than non-RI cases. In the present work, the RI and non-RI (neutral) values are approximately the same in the ATL basin (Table 4). With regard to the actual upper-level divergence magnitudes, our neutral value of $3.02 \times 10^{-6} \text{ s}^{-1}$ is similar to the KDK non-RI value of $2.63 \times 10^{-6} \text{ s}^{-1}$, while our RI value of $2.84 \times 10^{-6} \text{ s}^{-1}$ is about twice as small as the KDK 35-kt RI value of $5.07 \times 10^{-6} \text{ s}^{-1}$. One possible reason for this discrepancy is that we use filtered winds, which attempts to reduce the TC-induced outflow while keeping the larger-scale environmental divergence. However, the most likely reason is the use of 0–24-h averaging in KDK versus our analysis at the initial time. To put this in perspective with the composite TC life cycle shown in Fig. 4, our environmental parameters for RI are assessed at $t = -24$ h, while KDK results more closely resemble averages between $t = -24$ and $t = 0$ h. As TCs rapidly intensify, the TC-induced divergence will increase substantially in this time frame, which may explain why KDK finds larger upper-level divergence values than the present study. Similarly, as TCs weaken ($t = 0$ h in Fig. 4), the TC-induced upper-level divergence may very well remain large and then begin to decrease. It is difficult to remove the TC-induced component of the upper-level divergence (which is mostly attributed to the cumulus parameterization) from operational analysis due to its large scale. Since the TC-induced component of upper-level

divergence is positively correlated with TC intensity, it is possible to obtain different results if temporal averaging is used to compute this value. We feel our method of examining the environment at $t = 0$ h is justified because we wish to see how the TC responds to the environmental upper-level divergence, while minimizing the TC-induced effects on this field as it changes in intensity.

Another discrepancy between KDK and the present work is the magnitudes of the deep-layer shear. KDK finds shear values for non-RI and RI that are approximately 3 m s^{-1} less than our neutral and RI values, respectively (Table 5). However, both studies find ATL RI values of shear to be approximately 3 m s^{-1} less than non-RI. To understand if the filtering was the cause of some of these differences, the shear and divergence values were recalculated using the unfiltered 200-mb winds. By using unfiltered winds, the shear was reduced by approximately 2–3 m s^{-1} across all intensity change bins, causing the values to be closer to KDK. The upper-level divergence increased across all intensity change bins, and the new $10^\circ \times 10^\circ$ box average RI value ($9.68 \times 10^{-6} \text{ s}^{-1}$) was approximately 25% larger than the neutral ($7.65 \times 10^{-6} \text{ s}^{-1}$) value. Since the unfiltered winds include more TC-induced upper-level divergence, we feel that the filtered winds are more appropriate to use. It should also be noted that separation of the TC winds from the environmental winds at upper levels is not a trivial task, and there will be some uncertainty in the magnitudes of various parameters due to the particular filtering method that was chosen.

5. Environmental variability of rapidly intensifying TCs

By using the composite method, we have purposely focused on examining the average environment for each intensity change group. However, one may wonder about

the level of variability in the environment for various TCs undergoing various intensity changes. Considering the importance of understanding rapid intensification, in this section we examine the environmental variability for RI events. Do TCs rapidly intensify only when all the environmental parameters discussed here are very favorable? Or are there compensating factors, such as very weak shear compensating for marginal SSTs, or large instability compensating for strong shear?

To answer these questions, the variability in rapidly intensifying TCs in both basins was examined. Four environmental parameters were selected: deep-layer shear, SST, 200-hPa divergence, and instability. Then, scatterplots of RI storms in each basin were constructed to depict the variability in the environment for these storms in two-dimensional phase spaces from combinations of these parameters: (i) upper-level divergence versus deep-layer shear, (ii) upper-level divergence versus SST, (iii) SST versus deep-layer shear, and (iv) instability versus deep-layer shear. These plots are designed to illustrate some of the environmental variability that exists in RI storms.

The scatterplots are shown in Fig. 16. In both basins, upper-level divergence is found to be positively correlated with deep-layer shear, indicating that stronger upper-level divergence partially compensates for the detrimental effect of wind shear. In both basins, upper-level divergence was also found to be positively correlated with SST. This indicates that RI can happen over warm SSTs and strong upper-level divergence, as well as marginal SST and weaker upper-level divergence. In the latter case there may be some other compensating factor helping the TC rapidly intensify. In the WPAC, there was found to be no trend between SST and deep-layer shear, indicating that RI events happen over similar SSTs with varying levels of shear. In the ATL, however, SST was found to be positively correlated with deep-layer shear. This indicates that warmer SSTs partially compensate for the negative influence of deep-layer shear in the ATL to help storms rapidly intensify. In both basins, instability was negatively correlated with deep-layer shear. This indicates that RI events can happen in either high instability and weak shear environments, or lower instability and stronger shear environments. In the latter case, there must be other favorable compensating factors, either in the environment or internal dynamics.

To further illustrate the environmental variability, some individual TCs were also examined. In Table 6, three RI events were selected from each basin. In the ATL, the events of Katrina (0000 UTC 28 August 2005), Rita (0000 UTC 21 September 2005), and Wilma (0000 UTC 21 October 2005) were chosen. In the WPAC the chosen events were: Nesat (1200 UTC 31 May 2005), Chaba (0000 UTC 28 August 2004), and Sinlaku (0000 UTC

9 September 2008). The TC that had the most favorable environmental parameter is bolded for each basin. In the ATL, Katrina had the warmest SSTs, highest midlevel humidity, and largest instability. Rita had the weakest deep-layer shear and low-level relative humidity. Wilma had the largest low-level convergence, upper-level divergence, and low-level relative humidity. Based on these data, it can be inferred that the thermodynamic environment was quite favorable for Katrina, potentially helping it rapidly intensify, while more favorable dynamical forcing allowed Wilma to rapidly intensify. For the WPAC storms, Sinlaku had very weak shear, warm SSTs, large upper-level divergence, and higher midlevel relative humidity, helping it rapidly intensify. On the other hand, Chaba had the largest low-level convergence and low-level environmental relative vorticity in the group, helping it rapidly intensify. Nesat rapidly intensified in relatively marginal SSTs, but was aided by weak vertical wind shear.

The preceding analysis indicates there is a large amount of variability in the environment for TCs undergoing RI events, and in many cases there are compensating factors in which one very favorable environmental parameter makes up for a marginal one.

6. Conclusions

Tropical cyclone intensity change is regulated by conditions in the large-scale environment and ocean, as well as internal dynamical processes. This paper has been an effort to better quantify environmental control on TC intensity change, and in particular rapid intensification. The NOGAPS 0000 and 1200 UTC daily global analysis and TMI data were used in conjunction with the JTWC and NHC best-track data from 2003 to 2008 to assess the characteristics of TCs undergoing different intensity change episodes in both the western North Pacific (WPAC) and North Atlantic (ATL) ocean basins. A number of atmospheric variables were composited that are known to affect TC intensity change. Additionally, the best-track data was used to create climatology and persistence composites.

The differences in the environmental parameters between rapidly intensifying (RI) TCs and weakening, neutral, and intensifying TCs were quantified using statistical analysis. While some environmental differences were found between RI and weakening/neutral TCs in both basins, the environment of RI TCs and intensifying TCs was found to be quite similar, indicating that the rate of intensification is only weakly dependent on the environmental conditions, on average. Notable exceptions were that in the WPAC, rapid intensification events occurred in environments with significantly larger conditional

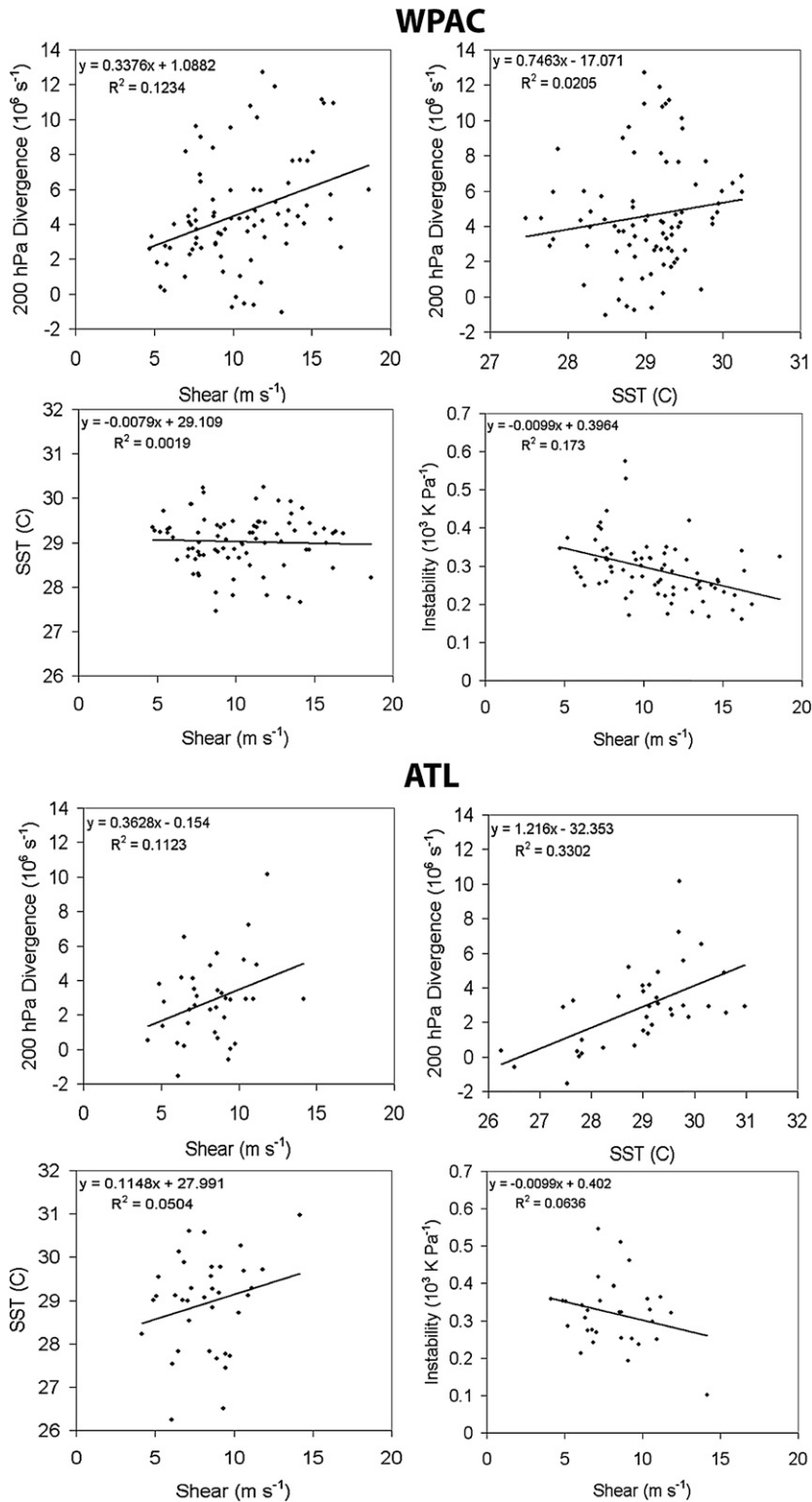


FIG. 16. Variability in environmental parameters for rapidly intensifying TCs in the (top) WPAC and (bottom) ATL basins.

TABLE 6. Variability in environmental parameters for a few TCs in the WPAC and ATL basins undergoing RI events. In each basin, the TC with the most favorable environmental parameter is set in boldface.

Quantity	Katrina 12L	Rita 18L	Wilma 25L	Nesat 4W	Chaba 19W	Sinlaku 15W
	ATL 2005 0000 UTC 28 Aug	ATL 2005 0000 UTC 21 Sep	ATL 2005 0000 UTC 18 Oct	WPAC 2005 1200 UTC 31 May	WPAC 2004 0000 UTC 28 Aug	WPAC 2008 0000 UTC 9 Sep
Deep-layer shear (m s^{-1})	10.46	6.49	10.63	8.71	12.89	7.91
SST ($^{\circ}\text{C}$)	30.27	30.13	29.69	28.84	29.03	30.24
850-hPa relative humidity (%)	74.47	81.53	80.10	83.28	83.34	81.68
500-hPa relative humidity (%)	62.04	54.52	55.73	68.04	68.51	77.07
850-hPa divergence (10^{-6} s^{-1})	-0.45	-2.01	-2.78	-1.34	-4.06	-2.82
200-hPa divergence (10^{-6} s^{-1})	2.91	6.52	7.24	5.40	4.58	6.86
$\partial\theta_E/\partial p$ (10^3 K Pa^{-1})	0.33	0.27	0.30	0.29	0.42	0.30
850-hPa vorticity (10^{-6} s^{-1})	9.98	1.92	21.89	11.50	17.02	15.28

instability than intensifying events. In the ATL, rapid intensification events occurred in environments with weaker deep-layer shear than intensifying events. An important finding of this work is that SSTs are initially similar between intensifying and rapidly intensifying TCs. These results indicate that on average, if TC moves over a warm ocean anomaly, it is equally likely to intensify slowly or rapidly, assuming all other atmospheric factors are equal and that the TC is moving fast enough that significant upwelling and mixing of cooler water does not occur.

With regard to the climatology and persistence variables, the significant differences are as follows. The TCs about to undergo an RI episode were more intense initially in both basins than the TCs about to undergo a neutral or intensifying episode. In the WPAC, RI, intensifying, and neutral storms had similar speeds, heading angles, and had similar average latitudes and longitudes. In the ATL, RI storms were located farther south than intensifying and neutral storms, moved faster, and had a more westward component to the heading.

In comparing the two ocean basins among the intensifying and RI categories, it was found that the WPAC had more favorable environment for TC intensification than the ATL, consistent with past work. The WPAC had warmer SSTs, greater low- and midlevel relative humidity, a greater areal extent and magnitude of large-scale low-level convergence and upper-level divergence, and low-level background relative vorticity. However, the ATL was found to have greater conditional instability and less deep-layer vertical wind shear. The more favorable environment in the WPAC explains why TCs in that basin intensify at a faster rate and achieve a higher maximum intensity (Fig. 4).

Based on this compositing study, it can reasonably be concluded that rapid intensification is mostly controlled by internal dynamical processes, provided that a preexisting favorable environment exists. These internal dynamical

processes are inherently less predictable, and therefore RI may never be well predicted by deterministic mesoscale models. These relative roles of internal and external processes (as well as scale interactions) in TC intensity change will be further tested using a full-physics mesoscale model in a hybrid idealized-real framework. These environmental composites will be used to construct realistic storm environments, and the role of internal dynamical processes in TC intensity change will be clarified.

Acknowledgments. This research was performed while the first author held a National Research Council Research Associateship Award at the U.S. Naval Research Laboratory in Monterey, California. The work was partially supported by ONR Grants N000140710145, N000140810256, PE0602435N, and NRL Subcontract N00173-06-1-07031. The International Pacific Research Center is partially sponsored by the Japan Agency for Marine-Earth Science and Technology (JAMSTEC), NASA (NNX07AG53G), and NOAA (NA17RJ1230). We are grateful for the constructive comments of three anonymous reviewers, which led to improvements in this manuscript.

REFERENCES

- Bender, M. A., and I. Ginis, 2000: Real-case simulations of hurricane-ocean interaction using a high-resolution coupled model: Effects on hurricane intensity. *Mon. Wea. Rev.*, **128**, 917–946.
- Black, P. G., and R. A. Anthes, 1971: On the asymmetric structure of the tropical cyclone outflow layer. *J. Atmos. Sci.*, **28**, 1348–1366.
- Bosart, L. F., C. S. Velden, W. E. Bracken, J. Molinari, and P. G. Black, 2000: Environmental influences on the rapid intensification of Hurricane Opal (1995) over the Gulf of Mexico. *Mon. Wea. Rev.*, **128**, 322–352.
- Cecil, D. J., and E. J. Zipser, 1999: Relationships between tropical cyclone intensity and satellite-based indicators of inner-core convection: 85-GHz ice-scattering signature and lightning. *Mon. Wea. Rev.*, **127**, 103–123.

- Challa, M., and R. L. Pfeffer, 1980: Effects of eddy fluxes of angular momentum on model hurricane development. *J. Atmos. Sci.*, **37**, 1603–1618.
- Charney, J. G., and A. Eliassen, 1964: On the growth of the hurricane depression. *J. Atmos. Sci.*, **21**, 68–75.
- Daley, R., and E. Barker, 2001: NAVDAS: Formulation and diagnostics. *Mon. Wea. Rev.*, **129**, 869–883.
- DeMaria, M., 1996: The effect of vertical shear on tropical cyclone intensity change. *J. Atmos. Sci.*, **53**, 2076–2087.
- , J. A. Knaff, and C. Sampson, 2007: Evaluation of long-term trends in tropical cyclone intensity forecasts. *Meteor. Atmos. Phys.*, **97**, 19–28.
- Dvorak, V. F., 1975: Tropical cyclone intensity analysis and forecasting from satellite imagery. *Mon. Wea. Rev.*, **103**, 420–430.
- , 1984: Tropical cyclone intensity analysis using satellite data. NOAA Tech. Rep. NESDIS 11, 47 pp.
- Elsberry, R. L., W. M. Frank, G. J. Holland, J. D. Jarrell, and R. L. Southern, 1987: *A Global View of Tropical Cyclones*. University of Chicago Press, 192 pp.
- , T. D. B. Lambert, and M. A. Boothe, 2007: Accuracy of Atlantic and eastern North Pacific tropical cyclone intensity forecast guidance. *Wea. Forecasting*, **22**, 747–762.
- Emanuel, K., 1986: An air–sea interaction theory for tropical cyclones. Part I: Steady-state maintenance. *J. Atmos. Sci.*, **43**, 585–604.
- , 1988: The maximum intensity of hurricanes. *J. Atmos. Sci.*, **45**, 1143–1155.
- , 2000: A statistical analysis of tropical cyclone intensity. *Mon. Wea. Rev.*, **128**, 1139–1152.
- Flatau, M., W. H. Schubert, and D. E. Stevens, 1994: The role of baroclinic processes in tropical cyclone motion: The influence of vertical tilt. *J. Atmos. Sci.*, **51**, 2589–2601.
- Frank, W. M., and E. A. Ritchie, 2001: Effects of vertical wind shear on the intensity and structure of numerically simulated hurricanes. *Mon. Wea. Rev.*, **129**, 2249–2269.
- Goerss, J. S., and R. A. Jeffries, 1994: Assimilation of synthetic tropical cyclone observations into the Navy Operational Global Atmospheric Prediction System. *Wea. Forecasting*, **9**, 557–576.
- Gray, W. M., 1968: Global view of the origin of tropical disturbances and storms. *Mon. Wea. Rev.*, **96**, 669–700.
- Guimond, S. R., G. M. Heymsfield, and F. J. Turk, 2010: Multiscale observations of Hurricane Dennis (2005): The effects of hot towers on rapid intensification. *J. Atmos. Sci.*, **67**, 633–654.
- Hendricks, E. A., M. T. Montgomery, and C. A. Davis, 2004: The role of “vortical” hot towers in the formation of Tropical Cyclone Diana (1984). *J. Atmos. Sci.*, **61**, 1209–1232.
- , W. H. Schubert, R. K. Taft, H. Wang, and J. P. Kossin, 2009: Life cycles of hurricane-like vorticity rings. *J. Atmos. Sci.*, **66**, 705–722.
- Hilburn, K. A., and F. J. Wentz, 2008: Intercalibrated passive microwave rain products from the Unified Microwave Ocean Retrieval Algorithm (UMORA). *J. Appl. Meteor. Climatol.*, **47**, 778–794.
- Hogan, T. F., and T. E. Rosmond, 1991: The description of the Navy Operational Global Atmospheric Prediction System’s spectral forecast model. *Mon. Wea. Rev.*, **119**, 1786–1815.
- Holland, G. J., 1997: The maximum potential intensity of tropical cyclones. *J. Atmos. Sci.*, **54**, 2519–2541.
- Hong, X., S. W. Chang, S. Raman, L. K. Shay, and R. Hodur, 2000: The interaction between Hurricane Opal (1995) and a warm core ring in the Gulf of Mexico. *Mon. Wea. Rev.*, **128**, 1347–1365.
- Hoshino, S., and T. Nakazawa, 2007: Estimation of tropical cyclone’s intensity using TRMM/TMI brightness temperature data. *J. Meteor. Soc. Japan*, **85**, 437–454.
- Jarvinen, B. R., C. J. Neumann, and M. A. S. Davis, 1984: A tropical cyclone data tape for the North Atlantic basin, 1886–1983: Contents, limitations, and uses. NOAA Tech. Memo. NWS/NHC 22, 21 pp. [Available from NOAA/NWS/NHC, Miami, FL 33165.]
- Jones, S. C., 1995: The evolution of vortices in vertical shear. I: Initially barotropic vortices. *Quart. J. Roy. Meteor. Soc.*, **121**, 821–851.
- Kaplan, J., and M. DeMaria, 2003: Large-scale characteristics of rapidly intensifying tropical cyclones in the North Atlantic basin. *Wea. Forecasting*, **18**, 1093–1108.
- , —, and J. Knaff, 2010: A revised tropical cyclone rapid intensification index for the Atlantic and eastern North Pacific basins. *Wea. Forecasting*, **25**, 220–241.
- Kossin, J. P., and W. H. Schubert, 2001: Mesovortices, polygonal flow patterns, and rapid pressure falls in hurricane-like vortices. *J. Atmos. Sci.*, **58**, 2196–2209.
- Lander, M. A., 1994: Description of a monsoon gyre and its effects on the tropical cyclones in the western North Pacific during August 1991. *Wea. Forecasting*, **9**, 640–654.
- Lin, I.-I., C.-H. Chen, I. Pun, W. T. Liu, and C.-C. Wu, 2009: Warm ocean anomaly, air sea fluxes, and the rapid intensification of Tropical Cyclone Nargis (2008). *Geophys. Res. Lett.*, **36**, L03817, doi:10.1029/2008GL035815.
- Lonfat, M., F. D. Marks Jr., and S. S. Chen, 2004: Precipitation distribution in tropical cyclones using the Tropical Rainfall Measuring Mission TRMM Microwave Imager: A global perspective. *Mon. Wea. Rev.*, **132**, 1645–1660.
- Mainelli, M., M. DeMaria, L. K. Shay, and G. Goni, 2008: Application of oceanic heat content estimation to operational forecasting of recent Atlantic category 5 hurricanes. *Wea. Forecasting*, **23**, 3–16.
- Mallen, K. J., M. T. Montgomery, and B. Wang, 2005: Reexamining the near-core radial structure for the tropical cyclone primary circulation: Implications for vortex resiliency. *J. Atmos. Sci.*, **62**, 408–425.
- McBride, J. L., and R. M. Zehr, 1981: Observational analysis of tropical cyclone formation. Part II: Comparison of non-developing versus developing systems. *J. Atmos. Sci.*, **38**, 1132–1151.
- Merrill, R. T., 1988a: Characteristics of the upper-tropospheric environmental flow around hurricanes. *J. Atmos. Sci.*, **45**, 1665–1677.
- , 1988b: Environmental influences on hurricane intensification. *J. Atmos. Sci.*, **45**, 1678–1687.
- Molinari, J., and D. Vollaro, 1989: External influences on hurricane intensity. Part I: Outflow layer eddy angular momentum fluxes. *J. Atmos. Sci.*, **46**, 1093–1105.
- , and —, 1990: External influences on hurricane intensity. Part II: Vertical structure and response for the hurricane vortex. *J. Atmos. Sci.*, **47**, 1902–1918.
- Montgomery, M. T., M. E. Nicholls, T. A. Cram, and A. B. Saunders, 2006: A vortical hot tower route to tropical cyclogenesis. *J. Atmos. Sci.*, **63**, 355–386.
- , N. V. Sang, and R. K. Smith, 2009: Do tropical cyclones intensify by WISHE? *Quart. J. Roy. Meteor. Soc.*, **135**, 1697–1714.
- Ooyama, K. V., 1964: A dynamical model for the study of tropical cyclone development. *Geofis. Int.*, **4**, 187–198.
- Peng, M. S., J. A. Ridout, and T. F. Hogan, 2004: Recent modifications of the Emanuel convective scheme in the Navy Operational Global Atmospheric Prediction System. *Mon. Wea. Rev.*, **132**, 1254–1268.

- Persing, J., M. T. Montgomery, and R. E. Tuleya, 2002: Environmental interactions in the GFDL hurricane model for Hurricane Opal. *Mon. Wea. Rev.*, **130**, 298–317.
- Reasor, P. D., M. T. Montgomery, and L. D. Grasso, 2004: A new look at the problem of tropical cyclones in vertical shear flow: Vortex resiliency. *J. Atmos. Sci.*, **61**, 3–22.
- , M. D. Eastin, and J. F. Gamache, 2009: Rapidly intensifying Hurricane Guillermo (1997). Part I: Low-wavenumber structure and evolution. *Mon. Wea. Rev.*, **137**, 603–631.
- Rogers, R., 2010: Convective-scale structure and evolution during a high-resolution simulation of tropical cyclone rapid intensification. *J. Atmos. Sci.*, **67**, 44–70.
- Rotunno, R., and K. A. Emanuel, 1987: An air-sea interaction theory for tropical cyclones. Part II: Evolutionary study using a nonhydrostatic axisymmetric numerical model. *J. Atmos. Sci.*, **44**, 542–561.
- Sang, N. V., R. K. Smith, and M. T. Montgomery, 2008: Tropical-cyclone intensification and predictability in three dimensions. *Quart. J. Roy. Meteor. Soc.*, **134**, 296–310.
- Schechter, D. A., M. T. Montgomery, and P. D. Reasor, 2002: A theory for the vertical alignment of a quasigeostrophic vortex. *J. Atmos. Sci.*, **59**, 150–168.
- Schubert, W. H., M. T. Montgomery, R. K. Taft, T. A. Guinn, S. R. Fulton, J. P. Kossin, and J. P. Edwards, 1999: Polygonal eyewalls, asymmetric eye contraction, and potential vorticity mixing in hurricanes. *J. Atmos. Sci.*, **56**, 1197–1223.
- Shapiro, L. J., and M. T. Montgomery, 1993: A three-dimensional balance theory for rapidly rotating vortices. *J. Atmos. Sci.*, **50**, 3322–3335.
- Vigh, J., and W. H. Schubert, 2009: Rapid development of the tropical cyclone warm core. *J. Atmos. Sci.*, **66**, 3335–3350.
- Wang, B., and X. Xie, 1996: Low-frequency equatorial waves in vertically sheared zonal flow. Part I: Stable waves. *J. Atmos. Sci.*, **53**, 449–467.
- Wang, Y., and C.-C. Wu, 2004: Current understanding of tropical cyclone structure and intensity changes—A review. *Meteor. Atmos. Phys.*, **87**, 257–278.
- Willoughby, H. E., J. A. Clos, and M. G. Shoreibah, 1982: Concentric eye walls, secondary wind maxima, and the evolution of the hurricane vortex. *J. Atmos. Sci.*, **39**, 395–411.
- Wingo, M. T., and D. J. Cecil, 2010: Effects of vertical wind shear on tropical cyclone precipitation. *Mon. Wea. Rev.*, **138**, 645–662.
- Zhang, F., and J. A. Sippel, 2009: Effects of moist convection on hurricane predictability. *J. Atmos. Sci.*, **66**, 1944–1961.